



Li₂CO₃ decomposition in Li-ion batteries induced by the electrochemical oxidation of the electrolyte and of electrolyte impurities

Anna T.S. Freiberg^{*}, Johannes Sicklinger, Sophie Solchenbach, Hubert A. Gasteiger

Chair of Technical Electrochemistry, Department of Chemistry and Catalysis Research Center, Technische Universität München, Garching, Germany

ARTICLE INFO

Article history:

Received 31 January 2020

Received in revised form

31 March 2020

Accepted 17 April 2020

Available online 18 April 2020

Keywords:

Lithium carbonate decomposition

Cathode surface impurity

On-line mass spectrometry

Electrolyte oxidation

Water oxidation in aprotic media

ABSTRACT

Layered lithium transition metal oxides are state-of-the-art cathode materials for Li-ion batteries. Nickel-rich layered oxides suffer from high surface reactivity toward ambient air. Besides hydroxides, carbonates are known to be the major surface impurities formed. While the decomposition of Li₂CO₃ in a battery cell has been studied extensively, the mechanistic aspects of its decomposition during cell formation/cycling are still highly controversial.

The decomposition reaction of Li₂CO₃ in a standard Li-ion battery electrolyte is studied by on-line electrochemical mass spectrometry, employing an electrode only consisting of Li₂CO₃ and conductive carbon. By modifying the electrode configurations in the cell, we are able to show that the decomposition of Li₂CO₃ occurs as a chemical process without any direct *electrochemical* oxidation of the Li₂CO₃ particles. Their decomposition proceeds by a *chemical* process via protons that are formed upon anodic oxidation of the electrolyte solvent and of trace impurities in alkyl carbonate based electrolytes. By adding common impurities in Li-ion battery electrolytes as ethanol and ethylene glycol, whose electrochemical oxidation at rather low anodic potentials (≈ 3.5 V vs Li⁺/Li) results in the formation of protons, the onset of CO₂ evolution from Li₂CO₃ is accordingly shifted to such low potentials. Tracing the proton-induced LiPF₆ decomposition products PF₅/POF₃, the formation of protons can be followed quantitatively and a direct correlation with the CO₂ produced by the proton-induced Li₂CO₃ decomposition is shown. Implications of these findings for transition metal oxide based cathode materials in Li-ion batteries are discussed based on the here found decomposition mechanism.

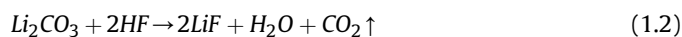
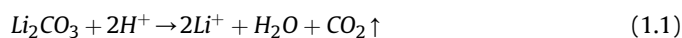
© 2020 The Authors. Published by Elsevier Ltd. This is an open access article under the CC BY-NC-ND license (<http://creativecommons.org/licenses/by-nc-nd/4.0/>).

1. Introduction

Layered lithium mixed transition metal oxides are state-of-the-art cathode materials for powering consumer electronics and battery electric vehicles [1,2]. Especially for large-scale manufacturing of batteries, the stability and robustness of the active material is of great importance for cost-efficient production [3,4]. The next-generation of layered transition metal oxides, namely so-called Ni-rich NCMs (Li_{1+δ}MO₂, with $\delta \approx 0.001$ –0.01 and M = Ni, Co, Mn), suffer from high surface reactivity toward ambient air [3,5,6], leading to significant surface resistances [3,7,8] and to severe gassing upon cycling [9]. Besides hydroxides, carbonates are the major surface impurities formed during exposure to the ambient

and during synthesis, in particular lithium carbonate [7,10,11], so that many previous studies have examined Li₂CO₃ decomposition in a Li-ion battery, whereby its detailed mechanism and its impact upon cycle-life are still disputed.

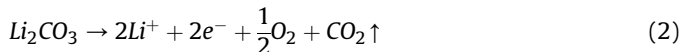
The decomposition mechanisms for Li₂CO₃ in an operating Li-ion battery suggested in the literature range from chemical decomposition [12], over electrochemical oxidation in parallel with that of the electrolyte solvent [13], all the way to the electrochemical oxidation of crystalline Li₂CO₃ with singlet oxygen release [14]. The proposed *chemical* decomposition of Li₂CO₃ in the presence of protons or other protic species like HF is described by equations (1.1) and (1.2).



^{*} Corresponding author.

E-mail address: anna.freiberg@tum.de (A.T.S. Freiberg).

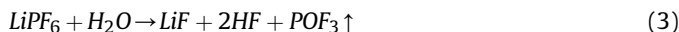
Alternatively, the *electrochemical* oxidation of Li_2CO_3 has been envisioned to proceed according to equation (2):



While all gassing analysis studies on the decomposition of Li_2CO_3 show the formation of CO_2 , the evolution of gaseous O_2 had not been observed. Therefore, in several studies, the lack of O_2 evolution in the proposed *electrochemical* oxidation of Li_2CO_3 acc. to equation (2) was ascribed to the formation of a highly reactive “nascent” oxygen species (O_2^*) that would be completely consumed by reaction with the organic electrolyte [14,15]. While there is a large number of “nascent” oxygen species that could be formed, specifically singlet oxygen has been suggested, as it is known to form in $\text{Li}-\text{O}_2$ batteries upon anodic polarization [16,17]. Even though we have recently shown that singlet oxygen is also reactive toward electrolyte solvents commonly used in Li-ion battery electrolytes [18], the complete absence of O_2 gas formed upon Li_2CO_3 decomposition is puzzling for the following reason. The major decay mechanism for singlet oxygen in solution is physical quenching, whereby the excitation energy of the singlet state is dissipated into vibrational modes of the solvent molecules, generating triplet oxygen [19]. As the latter does not strongly react with the commonly used cyclic and linear carbonates in Li-ion battery electrolytes, one would expect the detection of at least some triplet O_2 by on-line gas analysis if the Li_2CO_3 decomposition were to follow equation (2). A direct proof of the formation of singlet oxygen in this reaction is not possible in this case, as the characteristic photon emission at 634 nm would imply triplet O_2 gas to be detected [20]. Only chemical probes could be used to verify the presence of singlet oxygen or other nascent oxygen species, but they are typically unstable at the high anodic cathode potentials in Li-ion batteries; furthermore, their selectivity in an operating Li-ion battery is somewhat questionable. Another intriguing result with regards to the decomposition of Li_2CO_3 is a gassing study conducted in an all-solid-state Li-ion battery system by Bartsch et al. [21] While the complete decomposition of the native Li_2CO_3 film on layered transition metal oxides has been observed for liquid electrolytes over the course of the first few cycles [22,23], in the all-solid-state system only a minor fraction (7%) of the Li_2CO_3 was found to decompose to CO_2 gas [21]. This is unexpected if the observed Li_2CO_3 decomposition were to follow the *electrochemical* oxidation pathway acc. to equation (2), in which case the type of the electrolyte should have no impact. On the other hand, if the decomposition of Li_2CO_3 were to proceed by a *chemical* pathway acc. to equation (1.1) or (1.2), a significant reduction of protic species by switching to the all-solid-state electrolyte system could explain the limited decomposition of Li_2CO_3 in this case.

What can be assumed is that any “nascent” oxygen species that is reacting with the electrolyte solvent would initiate a decomposition reaction of the electrolyte that would likely lead to additional gassing. A detailed analysis of the gassing behavior might therefore be able to differentiate between the two most commonly proposed Li_2CO_3 decomposition pathways described above. The fact that only the *electrochemical* Li_2CO_3 oxidation in equation (2) will provide additional capacity is a strong differentiator as well. Regarding the proposed *chemical* decomposition reaction of Li_2CO_3 (equation (1.1) or (1.2)), the proton source is obviously an important factor. To the best of our knowledge, there is no detailed mechanistic study of the decomposition of Li_2CO_3 in standard Li-ion battery electrolytes composed of a mixture of organic carbonate solvents and LiPF_6 as conductive salt. The basic reactions of the LiPF_6 salt with water and protons are summarized in equations (3) and (4), whereby HF would be expected to be formed from the reaction of LiPF_6 with

either water or protons [24]:



The relevance of the decomposition of Li_2CO_3 impurities introduced by the cathode active material into Li-ion batteries from an application point of view can be illustrated by the following example: a high-energy density Li-ion battery pouch cell with a nominal capacity of 5 Ah would contain roughly 25 g of Ni-rich NCM (assuming $\approx 200 \text{ mAh/g}_{\text{NCM}}$) in a pouch cell with a total volume of 48 ml_{cell}. A Ni-rich cathode active material powder or electrode sheet can easily contain on the order of 0.3–0.6%_{wt} of Li_2CO_3 , either in the as-received material (e.g., 0.3%_{wt} reported for an NCA with 80% Ni [10] or 0.6%_{wt} reported for an NCM with 85% Ni [11]) or upon reaction with ambient air (e.g., 0.3%_{wt} after 3 months ambient storage of an NCM with 80% Ni [7]). Assuming 1 mol of CO_2 to be formed from every 1 mol of Li_2CO_3 acc. to equations (1) and (2), the estimated ≈ 0.075 – 0.15 g of Li_2CO_3 in such a pouch cell would result in the formation of the ≈ 25 – $50 \text{ cm}^3_{\text{std}}$ of CO_2 (referenced to 1 bar and 25 °C) only by these reactions, corresponding to an increase of the original cell volume by ≈ 52 – 104% . If this amount of gas were to be formed after the degassing step following the formation of the pouch cell, a substantial bulging of the cell would occur.

In this study we analyze the decomposition mechanism of Li_2CO_3 in a standard Li-ion battery electrolyte during the first anodic polarization of a carbon black based working electrode (WE) that is assembled together with a carbon/ Li_2CO_3 composite coated on a polymer separator. The decomposition pathway of Li_2CO_3 in a Li-ion battery cell is then examined by means of altering the carbon/ Li_2CO_3 composite configuration so that it is either in electronic contact with the carbon black WE or electronically isolated from the carbon black WE. This is supported by monitoring the gaseous products from electrolyte and Li_2CO_3 decomposition as a function of potential by means of on-line electrochemical mass spectrometry (OEMS) with both a one-compartment cell set-up [25] and a two-compartment set-up [22]. Further insights by OEMS analysis will be gained by using ^{13}C labeled Li_2CO_3 in the carbon/ Li_2CO_3 composite. Finally, by deliberately adding commonly encountered protic impurities in Li-ion battery solvents (viz., ethanol and ethylene glycol) to the electrolyte, the Li_2CO_3 decomposition mechanism occurring in a Li-ion battery can be established.

2. Experimental section

2.1. Preparation and characterization of the working electrodes

This work employs four different types of working electrodes (WEs), bonded with polyvinylidene fluoride (PVdF, Kynar HSV900, Arkema, France), that were used for the OEMS experiments. All electrodes were transferred into an Ar-filled glovebox without exposure to air for cell assembly ($<0.3 \text{ ppm O}_2$, $<0.1 \text{ ppm H}_2\text{O}$, MBraun, Germany). Please note, that the effect of binder content on the electrochemical response of the bare C65 WE was thoroughly studied, and no difference with respect to the extent of electrolyte oxidation capacity was found. The comparably high amount of PVdF used in this study does not alter the amount of surface area of carbon exposed to the electrolyte and does not lead to additional overpotentials. It shall also be noted that the presence of Li_2CO_3 in all composite electrodes does not lead to enhanced resistivity due to the maintained conductive pathway formed by the C65 network.

Conductive carbon WE: Super C65 (BET = $63 \text{ m}^2/\text{g}$, Timcal, Switzerland) working electrodes were prepared at ambient air by

mixing the carbon powder with PVdF at a mass ratio of 1:1 in NMP. Mixing was done in a planetary centrifugal mixer (Thinky, USA) at 2000 rpm for 10 min. The slurry was coated onto a stainless steel mesh (SS316, aperture 26 μm , wire diameter 25 μm , The Mesh Company Ltd, UK) using a gap-bar with a 450 μm gap. After drying at 60 °C overnight, the sheet was punched into 15 mm diameter electrodes, which were dried in a sealed glass oven under dynamic vacuum at 120 °C for 3 days. The final C65 mass of each of the electrodes was 2.7 ± 0.2 mg.

C65+Li₂CO₃ WEs with ball-milled lithium carbonate: For the preparation of C65/Li₂CO₃ composites, the particle size of the as-received Li₂CO₃ (>99%, Sigma Aldrich) was milled down using the following ball-milling procedure in order to obtain more intimately mixed composites. For this, 3 g of as-received Li₂CO₃ were dried at 300 °C for 3 days under dynamic vacuum in a sealed glass oven (Büchi, Switzerland) and transferred into an Ar-filled glovebox without exposure to air. In the glovebox (O₂ < 1 ppm, H₂O < 1 ppm; Jacomex, France), the dried Li₂CO₃ powder was first ground with an agate mortar and then given into an airtight ball-milling ZrO₂ beaker together with ZrO₂ beads of 2 mm diameter and 3 ml of N-methyl-2-pyrrolidone (NMP, Sigma Aldrich, 99.5%, dried over mole sieve, <5 ppm H₂O). An overall milling time of 2 h at 400 rpm, 2 h at 800 rpm, and 4 h at 1400 rpm was executed using a Fritsch pulverisette 7 ball-mill (Fritsch, Germany), with several breaks to prevent extensive heating. A particle size of 50–350 nm of Li₂CO₃ was therewith obtained, as observed by transmission electron microscopy (not shown). The mixture of Li₂CO₃ and NMP was then transferred back into the glovebox and given into a special accessory vessel for ultrasonic treatment, in which it was dispersed with an ultrasonic horn under Ar atmosphere (Branson 250 digital probe-sonifier). After 5 min, Super C65 and polyvinylidene fluoride (PVdF, Kynar HSV900, Arkema, France) at a mass ratio of 1:1:2 (Li₂CO₃: Super C65: PVdF) were added and sonicated for 5 more minutes. The resulting ink was coated in the glovebox onto a polyester separator (23 μm , FS23146, Freudenberg, Germany) using a 50 μm 4-edge blade, and then dried overnight at room temperature. Finally, electrodes of 15 mm diameter were punched inside the glovebox using a precision punch. The electrodes were transferred into a sealed glass oven without exposure to air and dried at 120 °C for 3 days under dynamic vacuum. The final Li₂CO₃ mass in each of the electrodes was 0.60 ± 0.07 mg. The electrodes will be further referred to as C65+Li₂CO₃.

C65+Li₂¹³CO₃ WEs: By an analogous procedure, composite electrodes of C65 but with isotopically labeled Li₂¹³CO₃ (>98%, >99% isotopic purity, Sigma Aldrich) at a mass ratio of 1:1 were prepared by transferring the powders into the glovebox after drying them at 300 °C under vacuum for 3 days in a sealed glass oven. In the glovebox, the powders were mixed in an agate mortar and an ink was prepared using the above described ultrasonic treatment. Coating and drying was executed as for the milled Li₂¹²CO₃, resulting in a comparable Li₂¹³CO₃ mass in each electrode of 0.63 ± 0.05 mg. The electrodes will be further referred to as C65+Li₂¹³CO₃.

C65@Li₂CO₃ WEs prepared by a precipitation route: The C65+Li₂CO₃ and C65+Li₂¹³CO₃ composite electrodes represent a physical mixture of still comparably large Li₂CO₃ particles (50–350 nm), which still may not allow for a sufficiently intimate contact with the conductive carbon that is required for an efficient charge transfer in case of a possible electrochemical oxidation reaction. Seeking to achieve a more realistic configuration, namely that of a thin carbonate layer formed on the surface of a Li-ion battery cathode active material by reaction with ambient air, a wet-impregnation technique was used to deposit a thin layer of Li₂CO₃ on the conductive carbon. The aim was a Li₂CO₃/carbon mass ratio of 3/7, which would correspond to a conceptual layer

thickness of 2–3 nm on the C65 carbon, and which would thus be similar to the approximate carbonate layer thickness formed on Ni-rich NCM after one year of storage in ambient air [7]. A saturated solution of Li₂CO₃ in ultrapure water (>15 M Ωcm , MilliQ, Merck, Germany) was prepared at room temperature. The corresponding amount of Super C65 powder was added and the slurry was stirred overnight. Afterwards, the water was evaporated in a rotary evaporator at 40 °C under dynamic vacuum. After 2 h, a dry homogeneous powder without white precipitates was obtained and further dried in a sealed glass oven under vacuum at 150 °C for 5 days. After drying, the powder was transferred into an Ar-filled glovebox and an ink was prepared following the procedure described for the C65+Li₂¹³CO₃ electrodes. The electrodes will be further referred to as C65@Li₂CO₃.

Physical-chemical characterization of the WEs: The mass ratio of C65 and Li₂CO₃ for all mixtures was verified by thermogravimetric analysis (TGA) of the powders in purified air up to 1000 °C, using a Mettler Toledo TGA/DSC 1 (Mettler Toledo, US). For this, roughly 10 mg of a powder sample of the C65/Li₂CO₃ composites (before the mixing step with PVdF in NMP) was given into an aluminum oxide crucible with minimized exposure to air (<1 min), which was then placed into the TGA sample chamber. After flushing the TGA chamber first with argon (100 ml/min) for 10 min and then for 5 min with purified air (40 ml/min) at room temperature, the sample was heated at 10 K/min from 25 °C to 1000 °C under a constant flow of air (20 ml/min) mixed with argon (20 ml/min). References of pure C65 and pure ball-milled Li₂CO₃ (referred to as Li₂CO₃ – milled) were measured as well.

The C65/Li₂CO₃ composite powders (C65+Li₂CO₃ and C65@Li₂CO₃) were further analyzed by X-ray diffraction (XRD), whereby the powders were sealed into 0.3 mm borosilicate capillaries (Hilgenberg GmbH, Germany). The measurements were conducted with a STOE STADI P diffractometer (STOE, Germany) in transmission mode, using Cu-K α_1 radiation ($\lambda = 1.54059$ Å, 50 kV, 30 mA, Ge (111) monochromatized) and a Mythen 1K detector (Dectris Ltd., Switzerland) with one data point every 0.012°/2 θ and a step time of 20 s. XRD measurements were conducted over night (≈ 13 h) in a 2 θ range of 15–88.2°.

2.2. Preparation of the counter electrodes

Partially delithiated LiFePO₄ (LFP) was used as counter electrode in the first set of experiments, i.e., for all one-compartment cell measurements. For this, LFP powder (BASF, Germany) was partially delithiated to an SOC of 90% (corresponding to Li_{0.1}FePO₄) using K₂S₂O₈ as oxidizing agent, as described earlier [16]. The Li_{0.1}FePO₄ powder was dried at 300 °C under vacuum in a sealed glass oven for 3 days before usage. LFP was then mixed with C65, VGCF-H (Showa Denko, Japan), and PVdF in a mass ratio of 90:2.5:2.5:5 in NMP using the planetary centrifugal mixer at 2000 rpm for 15 min. The ink was coated onto aluminum foil (18 μm , 99%, MTI, USA) using a gap-bar with a 450 μm gap. After drying at 60 °C overnight, electrodes of 17 mm diameter were punched and dried in a sealed glass oven under vacuum for 3 days at 120 °C and then transferred without air exposure into an Ar-filled glove box. The final mass and lithiation capacity of each of the electrodes was 55.5 ± 3.5 mg and 8.0 ± 0.5 mAh (assuming 90% lithiation capacity based on the specified full capacity of 160 mAh/g_{LFP}).

For the other set of experiments, i.e., for all two-compartment cell experiments, Li-metal was used as a counter electrode (450 μm thickness, 99.9% purity; Rockwood Lithium, USA), punched at a diameter of 17 mm.

2.3. OEMS measurements, ex-situ XPS analysis and galvanostatic experiments

The OEMS set-up using one- and two-compartment cells is described in earlier publications [22,25]. All measurements were executed at 25 °C.

One-compartment-cell OEMS measurements: For the first set of experiments, the one-compartment OEMS set-up was used in order to study the anodic oxidation capacity of the C65/Li₂CO₃ composite electrodes. A 90% delithiated LFP electrode (Li_{0.1}FePO₄) was used as counter electrode, which was covered by two 22 mm diameter glass-fiber separators (GF, 250 μm glass microfiber filter 691, VWR, Germany; dried for 3 days at 300 °C in a Büchi vacuum oven). Subsequently, 300 μl of 1 M LiPF₆ in a mixture of ethylene carbonate (EC) and ethyl-methyl carbonate (EMC) at a 3:7 mass ratio (LP57 electrolyte, BASF, Germany, < 5 ppm H₂O) were added.

For background measurements of the electrolyte oxidation reaction on a carbon surface, the C65 working electrode coated onto the stainless steel mesh was placed on top of the glass-fiber separators (see upper panel of the sketch in Fig. 3). To study the electrochemical oxidation of Li₂CO₃, the C65+Li₂CO₃ composite coated onto the polyester separator was added between the C65 working electrode and the glass-fiber separators, whereby the coated side is facing the C65 working electrode (see middle panel of the sketch in Fig. 3). This configuration provides electronic and ionic contact between the C65 working electrode and the C65/Li₂CO₃ composite, which would be required to allow for an electrochemical oxidation reaction (denoted as Li₂CO₃ electrode). Alternatively, to study the chemical oxidation of Li₂CO₃, the C65/Li₂CO₃ composite was sandwiched between the C65 working electrode and the glass-fiber separators such that the polyester separator of the C65/Li₂CO₃/separator assembly is facing the C65 working electrode, thereby electronically insulating the C65/Li₂CO₃ composite from the C65 working electrode (see lower panel of the sketch in Fig. 3), while maintaining ionic contact. In this configuration (denoted Li₂CO₃ interlayer), the Li₂CO₃ can only be decomposed chemically and not by electrochemical oxidation. Measurements of the thin Li₂CO₃ layer of the C65@Li₂CO₃ electrode was executed in the electrode configuration.

The electrochemical response of this kind of electrode stacking was studied thoroughly by coating a standard mixed transition metal layered oxide cathode active material (NCM111) onto a polyester separator and executing galvanostatic experiments in either electrode or interlayer configuration with a C65 WE, analogous to the measurements shown here. While in the interlayer configuration no capacity could be drawn from the active material, the potential profile and the achievable capacity in the electrode configuration was identical to a standard electrode configuration with the layered oxide material directly coated onto the mesh current collector. The stacking of electrodes as used in this study is therefore proven to give meaningful results without artefact arising from additional ohmic losses.

The cell assembled and sealed in an Ar-filled glovebox was transferred to the OEMS system, where a flow-restricting capillary is used to measure the gases evolved in the cell as a function of the applied potential. After a resting period of 4 h to allow extrapolation of the background of the mass spectrometer m/z signals, the working electrode potential was swept at 0.2 mV/s from its initial open circuit voltage (OCV) of ≈ 3.0 V vs Li⁺/Li (corresponding to a cell OCV of ≈ -0.4 V) to ≈ 5.5 V vs Li⁺/Li (corresponding to a cell voltage of ≈ 2.1 V). Reaching the upper potential limit, mass traces were recorded for another 2 h under OCV conditions. Quantification of the produced CO₂, CO, and O₂ gas was executed on the channels m/z = 44, 28, and 32, respectively, normalized to the

signal of the ³⁶Ar isotope to account for minor fluctuations in cell pressure and temperature (note that the m/z = 28 signal for CO was corrected by the contribution from CO₂ to this signal). For calibrations, the cell was flushed with a calibrated gas mixture (2000 ppm of each gas in Ar) after the measurement; for details see Metzger et al. [22] For the ex-situ XPS analysis of the cycled electrodes (see below), one set of measurements was conducted without a final exposure to the calibration gas.

Two-compartment-cell OEMS measurements: For the second set of experiments, the two-compartment OEMS set-up was used, employing a Li⁺-conducting glass-ceramic (LICGC, diameter 1 inch, thickness 150 μm, Ohara, Japan) that provides a gas-tight separation between the working and the counter electrode compartments [22]. This set-up was chosen to study the potential-dependent decomposition of deliberately added impurities that would already decompose at the potential of the partially delithiated LFP counter electrode in the one-compartment configuration; in addition, the two-compartment cell set-up also allows to quantitatively follow the gaseous LiPF₆ decomposition products. In the counter electrode compartment, a Li-metal electrode was used, which was covered with a 22 mm diameter glass-fiber separator filled with 150 μl of LP57 electrolyte; this compartment was then sealed with the LICGC inserted into an edge-seal to provide a gas-tight separation between the working and the counter electrode compartments.

In the working electrode compartment, 3 polyester separator disks (17 mm diameter, dried at 150 °C in a sealed glass oven under vacuum for 5 days) were placed onto the LICGC and filled with 200 μl of different types of electrolyte: (i) pure LP57, (ii) LP57 + 500 ppm ethanol (by weight, EtOH, 99.5% purity, dried over mole sieve, < 5 ppm H₂O, Sigma Aldrich), or (iii) LP57 + 350 ppm ethylene glycol (by weight, EG, 99.8% purity, dried over mole sieve, < 6 ppm H₂O, Sigma Aldrich). The working electrode was either a bare C65 working electrode or a C65 working electrode with an interlayer of milled C65+Li₂CO₃ or C65+Li₂¹³CO₃. The electrodes were placed so that the coated side is separated by the electrically insulating polyester separator from the C65 working electrode (interlayer configuration). After cell assembly in the Ar-filled glovebox, the cell was connected to the OEMS system. Following a resting period of 4 h, the working electrode potential was swept at 0.1 mV/s from its initial OCV of ≈ 3.0 V vs Li⁺/Li to 5.5 V vs Li⁺/Li; note that the scan rate was decreased due to the additional resistance caused by the added LICGC. Reaching the upper potential limit, mass traces were recorded for another 2 h under OCV conditions. Quantification of the produced CO₂, CO, and O₂ gas was executed as described above. The approximate concentration of PF₅ and POF₃ was determined by using the calibration factor reported by Solchenbach et al. at m/z = 85 [24], whereby this channel detects the sum of evolved PF₅ and POF₃ (referred to as "POF₃"). This is due to the fact that PF₅ evolved in the OEMS cell using our setup will always be detected as POF₃ at m/z = 85 (the strongest m/z signal for POF₃), caused by the high reactivity of PF₅ with the stainless steel parts of the cell and mass spectrometer inlet capillary (the same is likely the case for other setups used in battery research).

Ex-situ XPS measurements: The cycled C65/Li₂CO₃ interlayers from the one-compartment OEMS experiments were extracted from cells in an Ar-filled glovebox after the potential scan experiment, in which case no final exposure to the calibration gases was applied. Samples of 3 × 3 mm were cut from the interlayers and placed onto a stainless steel sample stub used for XPS measurements, including a reference interlayer that was not cycled. The sample stub was dried in a sealed glass oven under dynamic vacuum at room temperature overnight, and subsequently transferred in an inert transfer chamber (Kratos, UK) into the XPS interlock

without exposure to air. XPS spectra were recorded with an Axis Supra system (Kratos, UK) at a base pressure of $2 \cdot 10^{-8}$ Torr, using a monochromatic Al K α source (1486.6 eV). A pass energy of 20 eV, a step size of 0.1 eV, and a dwell time of 200 ms was chosen for a spot size of $800 \times 300 \mu\text{m}$. Binding energies were corrected based on the carbon signal at 284.8 eV in the C 1s spectrum. The C 1s region (296–280 eV B.E.) was recorded 5 times and averaged to ensure that all Li_2CO_3 was decomposed during the first anodic sweep in the OEMS measurement.

One-compartment-cell galvanostatic measurements: For the galvanostatic set of experiments, the one-compartment set-up was used in order to study the anodic oxidation capacity of the C65/ Li_2CO_3 composite electrodes and especially the electro-oxidation of water. A 90% delithiated LFP electrode ($\text{Li}_{0.1}\text{FePO}_4$) was used as counter electrode, which was covered by five polyester separator disks (22 mm diameter, dried at 150°C in a sealed glass oven under vacuum for 5 days). Subsequently, 200 μl of bare LP57 electrolyte (<5 ppm H_2O) or LP57 electrolyte spiked with 585 ppm H_2O were added. The amount of water was chosen based on the stoichiometric decomposition of Li_2CO_3 present in the cell to water that will dissolve in the electrolyte ($0.6 \text{ mg}_{\text{Li}_2\text{CO}_3} \hat{=} 8.12 \text{ mmol}_{\text{Li}_2\text{CO}_3} \hat{=} 8.12 \text{ mmol}_{\text{H}_2\text{O}} \hat{=} 585 \text{ ppm}_{\text{H}_2\text{O}}$). The working electrode set-up is as described for the one-compartment OEMS set-up. The electrolyte was spiked with water directly before cell assembly. The cell assembled and sealed in an Ar-filled glovebox was directly placed into a temperature controlled chamber at 25°C , connected to a multi-channel potentiostat (Biologic VMP3, France) and cycled galvanostatically. The time between mixing of the electrolyte and start of the electrochemical cycling was kept below 15 min in all cases. The C-rate was defined based on the average Li_2CO_3 amount in the cell assuming a 2-electron oxidation mechanism, which would correspond to a “capacity” of the cell of 0.435 mAh. The charge was executed at C/25 (i.e., 0.0174 mA) and C/2 (i.e., 0.218 mA) for 40 h.

3. Results and discussion

3.1. Characterization of the C65/ Li_2CO_3 composite powders by TGA and XRD

TGA measurements were conducted in order to verify the mass of Li_2CO_3 in all of the C65/ Li_2CO_3 composites. The results are shown in Fig. 1. The TGA measurements show the good agreement of the expected Li_2CO_3 weight fraction in the two composite materials C65+ Li_2CO_3 (mixture of ball-milled Li_2CO_3 and C65) and C65@ Li_2CO_3 (Li_2CO_3 wet-impregnation of C65). The slight weight loss at temperatures below the carbon oxidation onset (i.e., at $< 500^\circ\text{C}$) is caused by adsorbed water due to short exposure to air prior to the experiment. The weight loss until 550°C is caused by the complete oxidation of the C65 carbon to CO_2 , whereas the decomposition of Li_2CO_3 at roughly 720°C forms CO_2 and Li_2O [26].

In order to prove that a thin, amorphous Li_2CO_3 layer is formed on the C65 carbon in case of the C65@ Li_2CO_3 composite, X-ray diffractograms were recorded for the pure Li_2CO_3 powder before ball-milling, for the physical mixture of C65 and ball-milled Li_2CO_3 (C65+ Li_2CO_3), and for the material prepared by wet-impregnation of Li_2CO_3 on C65 carbon (C65@ Li_2CO_3). Fig. 2 shows that the distinct diffraction peaks of Li_2CO_3 (indicated by dashed-dotted vertical lines) are already less pronounced and broadened in case of the physical mixture of the ball-milled Li_2CO_3 with C65 (light blue line) and tend to completely disappear for the composite powder prepared by wet-impregnation (C65@ Li_2CO_3 , green line). Although the strong amorphous background of the C65 carbon black makes any quantification impossible, the lack of clear diffraction features for

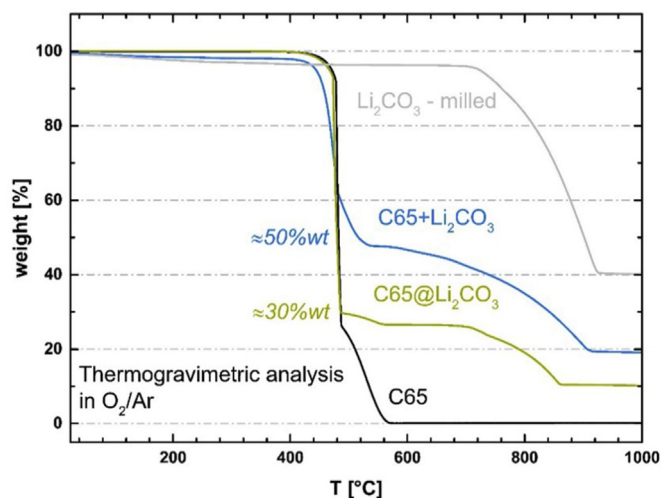


Fig. 1. Thermogravimetric analysis of the powders used for the preparation of Li_2CO_3 / C65 composite electrodes in $\approx 10\%$ O_2 in Ar at 10 K/min. The mass loss at roughly 500°C corresponds to the complete oxidation of the C65 carbon (illustrated by the reference experiment with pure C65, see black line), whereas Li_2CO_3 decomposition is starting at roughly 720°C (illustrated by the reference experiment for ball-milled Li_2CO_3 , see grey line).

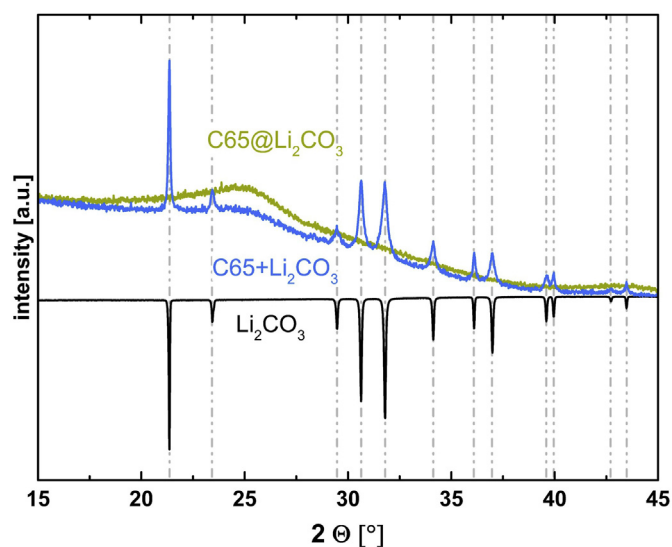


Fig. 2. X-ray diffractograms of C65/ Li_2CO_3 composites prepared by either mixing ball-milled Li_2CO_3 and C65 (C65+ Li_2CO_3 , light blue line) or by wet-impregnation of Li_2CO_3 on C65 (C65@ Li_2CO_3 , green line) in comparison to a Li_2CO_3 reference (black line). (For interpretation of the references to colour in this figure legend, the reader is referred to the Web version of this article.)

the C65@ Li_2CO_3 composite powder clearly indicates that an amorphous Li_2CO_3 layer is formed. While this of course provides no evidence that a thin Li_2CO_3 layer covering the surface of the C65 particles was obtained, it is a good indication that no large domains of Li_2CO_3 have been formed. Further imaging techniques such as SEM or TEM did not show any inhomogeneity of the sample, but owing to the poor contrast between carbon and Li_2CO_3 , differentiation of the two phases is also not possible by this means. Therefore, while we believe that the wet-impregnation process resulted in a more intimate contact between the carbon particles and Li_2CO_3 , we have been unable to prove this assumption.

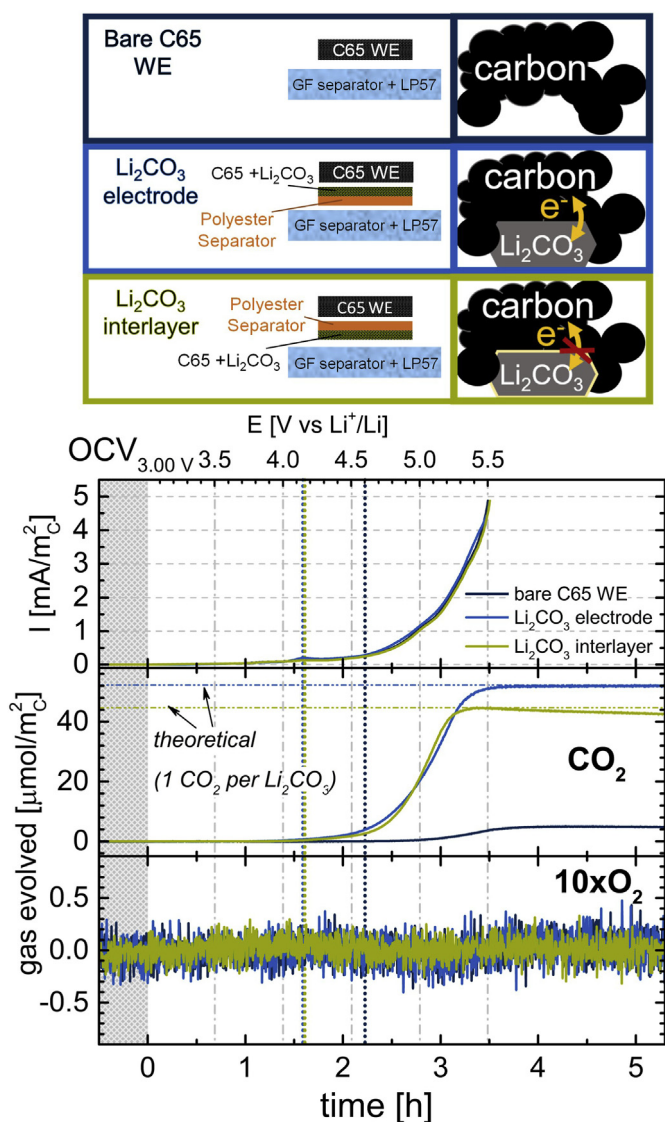


Fig. 3. Upper panel of the plots: Oxidation current density (normalized to the surface area of the C65 carbon that is in electrical contact with the C65 WE) for a linear potential scan (0.2 mV/s) of the working electrode (WE) potential from OCV (≈ 3.0 V vs Li^+/Li) to ≈ 5.5 V vs Li^+/Li for three different WE configurations with LP57 electrolyte in one-compartment OEMS cells. Middle/lower panels of the plots: Cumulative amount of evolved CO_2/O_2 referenced to the same carbon surface areas (solid lines), as determined from the OEMS channels $m/z = 44$ and $m/z = 32$, respectively; the horizontal dashed-dotted lines represent the maximum amount of CO_2 which could be derived from the (electro)chemical decomposition of Li_2CO_3 (assuming 1 mol CO_2 per mol of Li_2CO_3). Sketched WE configurations: bare C65 carbon WE (upper panel of the sketch and dark blue lines in the plots), C65 WE with a Li_2CO_3 electrode (middle panel of the sketch and light blue lines in the plots), and C65 WE with a Li_2CO_3 interlayer (lower panel of the sketch and green lines in the plots). (For interpretation of the references to colour in this figure legend, the reader is referred to the Web version of this article.)

Table 1
Comparison of the observed oxidation charge (Q_{ox} , normalized to the surface area of the C65 carbon that is in electrical contact with the C65 working electrode (WE)) accumulated over the course of a linear potential scan (0.2 mV/s) of the WE potential from OCV (≈ 3.0 V vs Li^+/Li) to ≈ 5.5 V vs Li^+/Li for three different WE configurations with LP57 electrolyte in one-compartment OEMS cells: a bare C65 carbon WE (upper panel of the sketch and dark blue lines in Fig. 3), a C65 WE with a Li_2CO_3 electrode (middle panel of the sketch and light blue lines), and a C65 WE with a Li_2CO_3 interlayer (lower panel of the sketch and green lines), both based on the C65+ Li_2CO_3 composite. The onset potential for CO_2 evolution and the conversion of Li_2CO_3 over the course of the potential scan are determined from the OEMS signal at $m/z = 44$ (assuming 1 mol CO_2 per mol of Li_2CO_3). The standard deviation from three independent repeat measurements is given as error range.

configuration	bare C65 WE	C65 WE + Li_2CO_3 electrode	C65 WE + Li_2CO_3 interlayer
Q_{ox} [$\text{mAh}/\text{m}^2\text{c}$]	2.31 ± 0.11	2.33 ± 0.12	2.20 ± 0.18
CO_2 onset potential	≈ 4.6 V vs Li^+/Li	≈ 4.2 V vs Li^+/Li	≈ 4.2 V vs Li^+/Li
Li_2CO_3 conversion	–	$95 \pm 2.2\%$	$97 \pm 1.3\%$

3.2. One-compartment OEMS data – electrochemical or chemical Li_2CO_3 decomposition?

The first question to be answered in this study is whether Li_2CO_3 can be *electrochemically* oxidized in a Li-ion battery environment. This will be examined by one-compartment OEMS measurements, using the various working electrode (WE) configurations described in the experimental section and illustrated by the three sketches in Fig. 3: (i) a bare C65 WE to quantify the electrochemical oxidation of the electrolyte on the conductive carbon surface (upper panel of the sketch); (ii) a C65+ Li_2CO_3 composite in electrical and ionic contact with the C65 WE (middle panel of the sketch) in order to quantify the extent of *electrochemical* oxidation of Li_2CO_3 in addition to electrochemical electrolyte oxidation (referred to as *Li₂CO₃ electrode* configuration, see Fig. 3); and, (iii) a C65+ Li_2CO_3 composite that is electrically isolated but in ionic contact with the C65 WE (lower panel of the sketch), the so-called *Li₂CO₃ interlayer* configuration, which allows for a *chemical* decomposition of Li_2CO_3 that might be caused by species produced by the electrochemical oxidation of the electrolyte at the C65 WE. The pertinent results of the experimental data shown in Fig. 3 are summarized in Table 1 (the given standard deviations are based on three independent repeat measurements).

The top panel of the plots in Fig. 3 shows the oxidation current during the anodic linear sweep of the WE potential at 0.2 mV/s from OCV (≈ 3.0 V vs Li^+/Li) to ≈ 5.5 V vs Li^+/Li . Note that the currents as well as the amount of evolved CO_2 and O_2 (middle/lower panels of the plots in Fig. 3) are normalized by the BET surface area of the C65 carbon in the C65 WE and in the Li_2CO_3 electrode; the C65 surface area in the Li_2CO_3 interlayer is excluded, as it is not in electrical contact with the C65 WE. The thus normalized current versus WE potential is essentially identical for all three electrode configurations, so that the overall oxidation charge, obtained by integration of the anodic current throughout the sweep from OCV to 5.5 V vs Li^+/Li , is also essentially identical within the experimental error (see first row in Table 1). The middle panel of the plot in Fig. 3 shows the cumulative CO_2 evolution normalized by the carbon surface area that is in electrical contact with the C65 WE (as described above). For the bare C65 WE (dark blue line), CO_2 evolution can be detected starting at ≈ 4.6 V vs Li^+/Li (marked by the dark blue dotted vertical line), gradually accumulating over the remainder of the potential scan up to 5.5 V vs Li^+/Li , and reaching a final maximum value of ≈ 5 $\mu\text{mol CO}_2/\text{m}^2\text{c}$. For the measurements with the C65+ Li_2CO_3 composites in both the Li_2CO_3 electrode configuration (light blue line) and the Li_2CO_3 interlayer configuration (green line), the onset of CO_2 evolution is shifted to a substantially lower potential of only ≈ 4.2 V vs Li^+/Li (marked by the light blue and green dotted vertical lines), whereby the CO_2 evolution rate is slow until a potential of ≈ 4.7 V is reached, after which the amount of accumulated CO_2 increases rapidly, until it levels off near the positive potential limit of 5.5 V vs Li^+/Li .

The overall amounts of CO_2 formed in the presence the C65+ Li_2CO_3 composites are significantly higher in comparison to

when only the C65 WE is used, a difference which we ascribe to the decomposition of Li_2CO_3 , as can be rationalized by the following consideration. Assuming a reaction stoichiometry of 1 mol of CO_2 produced per mol of Li_2CO_3 decomposed (acc. to equations (1) and (2)), the expected total amount of CO_2 (normalized again to the electrically connected C65 carbon surface area) can be predicted from the known amount of Li_2CO_3 in the cell (contained in the C65+ Li_2CO_3 composite). The thus predicted value is then added to the CO_2 amount stemming from electrolyte oxidation on the C65 WE (i.e., in the absence of the C65+ Li_2CO_3 composite, typically amounting to on the order of 10–20% of the amount calculated for the C65+ Li_2CO_3 composite), and this sum is marked by the horizontal dashed-dotted lines for the Li_2CO_3 electrode (light blue) and the Li_2CO_3 interlayer (green) configuration with the C65 WE. The measured total amount of evolved CO_2 at the end of the potential scan to 5.5 V vs Li^+/Li coincides astonishingly well with the predicted value in both cases, suggesting an essentially complete decomposition of Li_2CO_3 within the first anodic sweep. Please note that the difference in the predicted values stems from slight variations in the carbon loadings of the C65 working electrodes (major contributor to the carbon area to which all signals are normalized) as well as of the loadings of the C65/ Li_2CO_3 composites. The amount of Li_2CO_3 decomposition to CO_2 is deduced from these data by subtracting from the amount of CO_2 that is measured in the presence of the C65/ Li_2CO_3 composite that which is measured with the bare C65 WE, and then referencing this difference to the amount of CO_2 predicted from the known amount of Li_2CO_3 contained in the C65+ Li_2CO_3 composite; these values for the estimated conversion of Li_2CO_3 to CO_2 are listed in Table 1.

Despite the fact that the CO_2 evolution for the Li_2CO_3 electrode in combination with the C65 WE indicates an essentially complete decomposition of Li_2CO_3 to CO_2 by the end of the potential scan, the oxidation current vs potential and the total oxidation charge are essentially identical to that of the bare C65 electrode (see Fig. 3 and Table 1). This is inconsistent with the two-electron oxidation mechanism for Li_2CO_3 as proposed in the literature [14] (acc. to equation (2)), since the expected total charge contribution for the electrochemical oxidation of Li_2CO_3 in the Li_2CO_3 electrode would be $\approx 1.9 \text{ mAh/m}^2_{\text{C}}$, in addition to the total anodic charge observed for the bare C65 WE of $\approx 2.3 \text{ mAh/m}^2_{\text{C}}$ (see Table 1). Instead, the difference in the total anodic charge between these two electrode configurations (bare C65 WE vs C65 WE + Li_2CO_3 electrode) is within the error of independent repeat measurements (see Table 1). Furthermore, no evolution of O_2 is observed by OEMS (see lowest panel in Fig. 3), which is also inconsistent with an electrochemical oxidation of Li_2CO_3 acc. to equation (2). Thus, one can conclude that the electrochemical oxidation of Li_2CO_3 does not take place under these conditions.

In order to prove that Li_2CO_3 in the C65+ Li_2CO_3 composites is indeed completely decomposed after the potential scan to 5.5 V vs Li^+/Li , ex-situ XPS analysis was conducted. Fig. 4 shows the C1s region of the XPS spectra of the pristine C65+ Li_2CO_3 composites (dark blue line) in comparison to the C65+ Li_2CO_3 composites harvested from the OEMS cells after the potential scan to $\approx 5.5 \text{ V}$ vs Li^+/Li , where they had been used either in the Li_2CO_3 electrode configuration (light blue line) or in the Li_2CO_3 interlayer configuration (green line). The C1s spectrum of the pristine C65+ Li_2CO_3 composite consists of two main features, one that can be ascribed to carbon (C–C and C–H) at 284.8 eV and one that can be ascribed to carbonate (M– CO_3) around 289.9 eV. The latter is completely vanished in case of the C65+ Li_2CO_3 composites harvested after the OEMS measurements where they were configured as either Li_2CO_3 electrode or Li_2CO_3 interlayer. The small shoulder observed at 290.9 eV for the harvested C65+ Li_2CO_3 composites corresponds to non-volatile electrolyte decomposition products. This clearly

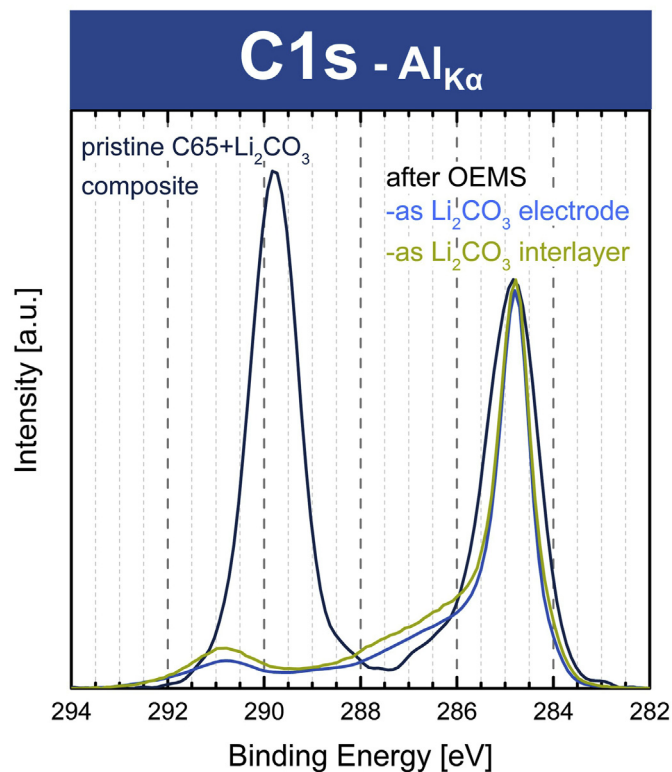


Fig. 4. C1s XPS spectra of the pristine C65+ Li_2CO_3 composite (dark blue line) and of the C65+ Li_2CO_3 composites scanned to $\approx 5.5 \text{ V}$ vs Li^+/Li either in the Li_2CO_3 electrode configuration (light blue line) or in the Li_2CO_3 interlayer configuration (green line), normalized to the peak of the conductive carbon. The strong M– CO_3 peak at roughly 289.8 eV B.E. is completely lost after the potential scan. (For interpretation of the references to colour in this figure legend, the reader is referred to the Web version of this article.)

proves the complete decomposition of all of the Li_2CO_3 in both the Li_2CO_3 electrode or Li_2CO_3 interlayer during the anodic scan to 5.5 V vs Li^+/Li shown in Fig. 3, a finding which is consistent with the above determined amount of evolved CO_2 for these two electrode configurations.

Though all experimental results indicate that Li_2CO_3 is not electrochemically oxidized in a Li-ion battery environment and instead is being decomposed chemically, the question remains on how accurately a physical mixture of large, μm -sized Li_2CO_3 particles might mimic a several nm thick carbonate layer that is formed natively on layered transition metal oxide based cathode active materials. In the hope of obtaining Li_2CO_3 particles/layers with more representative dimensions, a wet-impregnation technique was used in order to form a nominally 2–3 nm thick layer of Li_2CO_3 on the conductive carbon particles (denoted as C65@ Li_2CO_3 ; see experimental section). The current and the CO_2 evolution during a potential scan from OCV to $\approx 5.5 \text{ V}$ vs Li^+/Li recorded in a one-compartment cell for the C65@ Li_2CO_3 composite used in the Li_2CO_3 electrode configuration (i.e., the coating side facing the C65 WE) in comparison to the bare C65 electrode is shown in Fig. 5. Please note that the amount of evolved CO_2 for the experiment with the C65@ Li_2CO_3 composite in the Li_2CO_3 electrode configuration (Fig. 5b) is divided by a factor of 10.

Comparing the results from the C65@ Li_2CO_3 composite (Fig. 5b) to the background measurement with a bare C65 working electrode (Fig. 5a), the current drawn during the anodic potential sweep shown in the upper panel is not significantly altered by improving the electrical contact between the C65 carbon and the Li_2CO_3

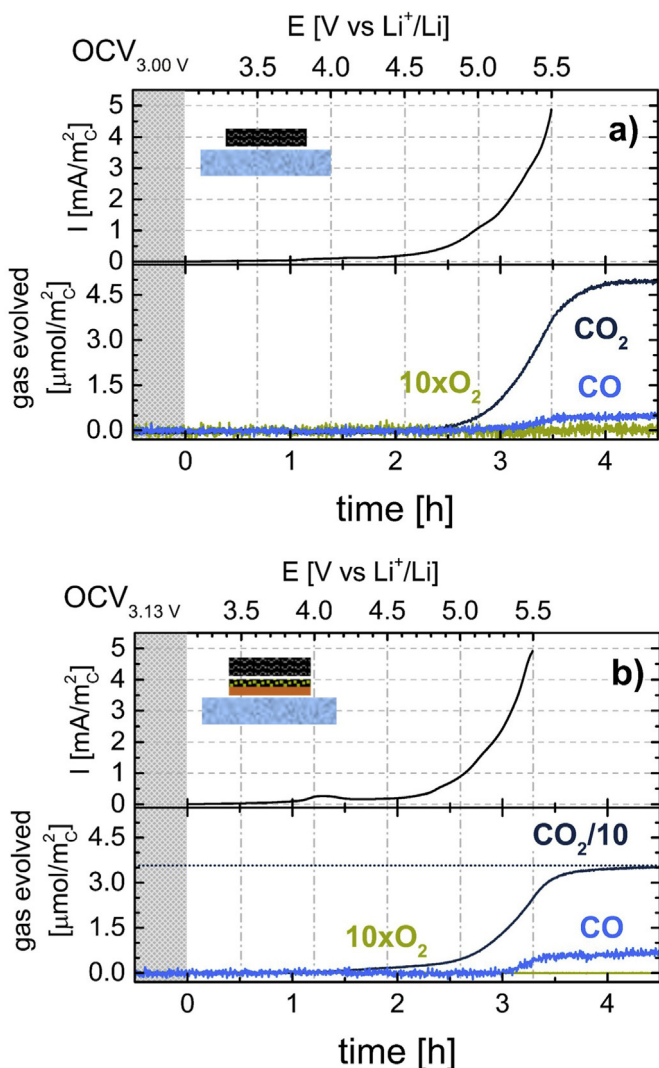


Fig. 5. Oxidation current density and gas evolution (normalized to the surface area of the C65 carbon that is in electrical contact with the C65 WE) for a linear potential scan (0.2 mV/s) of the working electrode (WE) potential from OCV (≈ 3.0 V vs Li^+/Li) to ≈ 5.5 V vs Li^+/Li for two different WE configurations (see sketches in the figure) with LP57 electrolyte in one-compartment OEMS cells: (a) on a bare C65 WE; (b) on a C65@ Li_2CO_3 composite in the Li_2CO_3 electrode configuration with a C65 WE. The anodic current is shown in the upper panels, while the cumulative amounts of evolved O_2 (green lines), CO (light blue lines), and CO_2 (dark blue lines) are shown in the bottom panels. The dotted horizontal line in the lower panel of (b) represents the expected CO_2 evolution for a 1:1 conversion of Li_2CO_3 to CO_2 , taking into account the CO_2 evolved from the C65 WE taken from the lower panel in (a). (For interpretation of the references to colour in this figure legend, the reader is referred to the Web version of this article.)

particles within the C65@ Li_2CO_3 composite. Also, the overpotential of both measurements are identical, meaning that even in case of the C65@ Li_2CO_3 composite, the conductive network of the carbon particles is not largely impacted by the amorphous Li_2CO_3 film formed, i.e., the film is not continuous. The additional CO_2 formed in the presence of the C65@ Li_2CO_3 composite in the Li_2CO_3 electrode configuration again essentially coincides with the expected value for a 1:1 conversion of Li_2CO_3 to CO_2 (see horizontal dotted line in Fig. 5b, that represents the sum of CO_2 formed by the anodic oxidation of the electrolyte and the expected CO_2 from Li_2CO_3 decomposition). The small additional anodic peak observed around 4 V vs Li^+/Li in Fig. 5 b is likely caused by the wet-impregnation technique that could lead to a higher residual water content of

the composite (hydrolysing the electrolyte), as excessive drying was avoided to not alter the morphology of the wet-impregnated Li_2CO_3 phase. As before, no evolution of O_2 is observed (not shown) and the characteristic profile of the CO evolution is also very similar; the slightly higher amount of CO could hint toward an increased moisture content, as discussed later.

To conclude, based on the one-compartment OEMS results, the decomposition of Li_2CO_3 in a Li-ion battery environment does not occur by an *electrochemical* oxidation reaction but by a *chemical* decomposition reaction, as Li_2CO_3 particles that are located in the vicinity of the working electrode can be fully decomposed in a single potential scan to ≈ 5.5 V vs Li^+/Li even in the absence of any electrical contact with the working electrode. An alternative mechanism would be that the Li_2CO_3 decomposes by a *chemical* reaction, namely by an acidic decomposition of Li_2CO_3 with either H^+ , HF, or other protic species, leading to CO_2 evolution and H_2O formation (see equations (1.1) and (1.2)). However, as the Li_2CO_3 decomposition is clearly potential dependent (see Figs. 3 and 5b), we propose that the onset potential for CO_2 evolution is an indirect measure of the formation of H^+ , HF, or other protic species by the oxidation of the electrolyte solvent and/or by organic electrolyte impurities. In order to further investigate this point, two-compartment OEMS experiments were conducted, so that electrolyte impurities could be added to the WE compartment without risking that they may be captured or transformed by the counter electrode. To furthermore avoid any interferences from the separator that must be placed onto the Li^+ -conducting glass on the working electrode side, a polyester separator was used instead of a glass-fiber separator, as the latter is known to react with, e.g., HF in the electrolyte.

3.3. Two-compartment OEMS data – chemical Li_2CO_3 decomposition mechanism

The question remains, whether the extent of electrolyte oxidation might be altered by the Li_2CO_3 decomposition, as the latter must form water as a by-product. Thus, it needs to be determined whether the additional CO_2 evolved in the presence of Li_2CO_3 stems entirely from Li_2CO_3 decomposition or whether (parts of) it derives from the chemical oxidation of the electrolyte solvent or from electrolyte impurities. In order to do so, a physical mixture of ^{13}C -labeled Li_2CO_3 (referred to as $\text{Li}_2^{13}\text{CO}_3$) and C65, i.e., a C65+ $\text{Li}_2^{13}\text{CO}_3$ composite, is used as interlayer in the two-compartment OEMS set-up. In this case, any $^{13}\text{CO}_2$ formed during the anodic potential scan must stem directly from the decomposition of $\text{Li}_2^{13}\text{CO}_3$, while any $^{12}\text{CO}_2$ above the background-level from the C65 WE must be caused by the electrochemical oxidation of the electrolyte. The presence of water, e.g., could increase the CO_2 evolution from the electrolyte at high anodic potentials [27]. The OEMS data for the C65+ $\text{Li}_2^{13}\text{CO}_3$ composite used in the $\text{Li}_2^{13}\text{CO}_3$ interlayer configuration are shown in Fig. 6b and compared with those of the bare C65 working electrode in Fig. 6a. Please note that the amount of evolved $^{13}\text{CO}_2$ from the $\text{Li}_2^{13}\text{CO}_3$ interlayer experiment is divided by 15 to fit onto the same scale.

Comparing the results obtained in the two-compartment OEMS set-up with a bare C65 working electrode (all $^{12}\text{CO}_2$ must come from electrolyte oxidation) in Fig. 6a with the results obtained with the additional $\text{Li}_2^{13}\text{CO}_3$ interlayer in Fig. 6b, it becomes clear that the overall amount of $^{12}\text{CO}_2$ formed upon the electrochemical oxidation of the electrolyte is not altered by the presence and decomposition of the $\text{Li}_2^{13}\text{CO}_3$ interlayer (dark blue lines in Fig. 6). As indicated by the dark red dotted horizontal line in Fig. 6b, the amount of $^{13}\text{CO}_2$ (dark red line) again coincides with the expected value based on a 1:1 conversion of $\text{Li}_2^{13}\text{CO}_3$ to $^{13}\text{CO}_2$. The only distinct difference that can be observed with regards to the impact

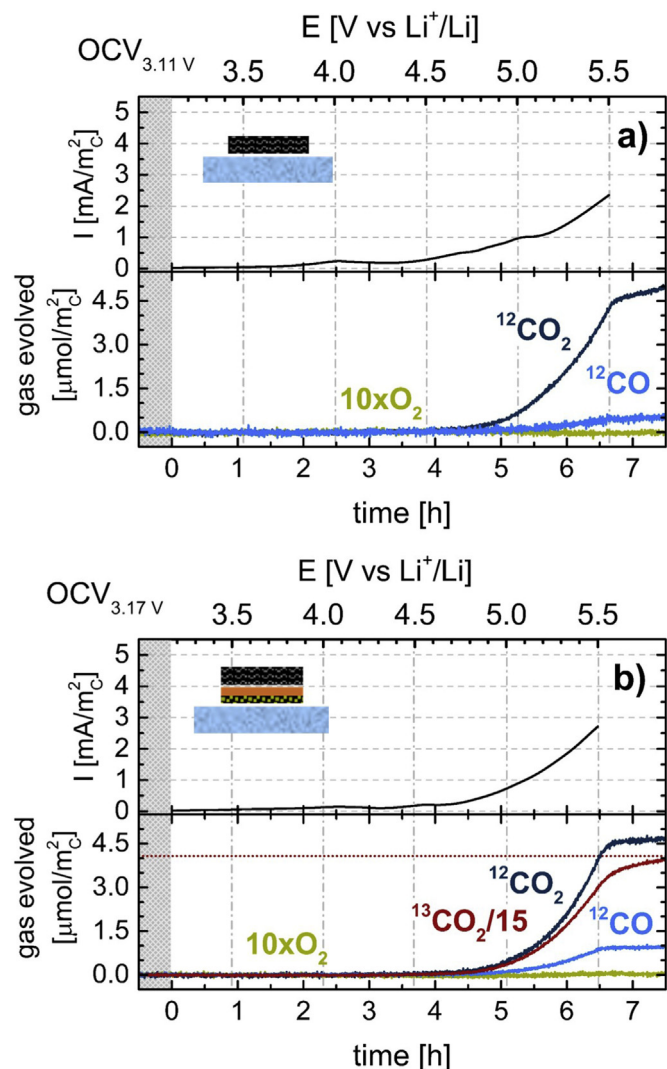


Fig. 6. Oxidation current density and gas evolution (normalized to the surface area of the C65 carbon that is in electrical contact with the C65 WE) for a linear potential scan (0.1 mV/s) of the working electrode (WE) potential from OCV (≈ 3.0 V vs Li⁺/Li) to ≈ 5.5 V vs Li⁺/Li for two different WE configurations (see sketches in the figure) with LP57 electrolyte in two-compartment OEMS cells: (a) on a bare C65 WE; (b) on a C65+Li₂¹³CO₃ composite in the Li₂¹³CO₃ interlayer configuration with a C65 WE. The anodic current is shown in the upper panels, while the cumulative amounts of evolved O₂ (green lines), ¹²CO (light blue lines), ¹²CO₂ (dark blue lines), and ¹³CO₂ (dark red line) are shown in the bottom panels. The dotted horizontal line in the lower panel of (b) represents the expected ¹³CO₂ evolution for a 1:1 conversion of Li₂¹³CO₃ to ¹³CO₂. (For interpretation of the references to colour in this figure legend, the reader is referred to the Web version of this article.)

of Li₂CO₃ decomposition on the electrolyte degradation is the ≈ 2 -fold higher amount of evolved ¹²CO that can be seen in Fig. 6b compared to that evolved in case of the bare C65 WE in Fig. 6a (light blue lines). Note that no ¹³CO is detected, which further confirms that the decomposition of Li₂CO₃ only leads to CO₂ as gaseous product. We know from earlier studies that enhanced water content of a carbonate based electrolyte will lead to the oxidation of carbon to CO₂ and CO at high potentials, as long as the water is truly present as H₂O (i.e., as long as it is not removed by reaction with the salt or the solvent) [27]. As in this case the water is formed in-situ by the chemical decomposition of Li₂CO₃, the reaction with the conductive salt LiPF₆ is apparently not fast enough to consume all the water, leaving enough residual H₂O in solution to react with the conductive carbon at high potentials. This is also accompanied by a

slightly higher oxidation current at potentials exceeding 5 V vs Li⁺/Li, as shown in Fig. 6b.

At this point it seems unambiguously clear that the decomposition of Li₂CO₃ in a Li-ion battery environment is not due to its *electrochemical* oxidation and that the Li₂CO₃ decomposition process has no direct impact on the decomposition of the electrolyte. The observation that Li₂CO₃ decomposition only occurs once a certain potential threshold is reached, can therefore only be explained by a reactive species that decomposes Li₂CO₃ and that is formed upon anodic oxidation. According to equation (1), these species are generally seen to be protons, as their reaction with inorganic carbonates is widely known. With respect to the formation of protons as reactive species, three main questions remain: (i) How could protons be generated in an aprotic Li-ion battery electrolyte? (ii) Can we trace the formation of protons during the anodic potential sweep? (iii) Can we influence the onset potential of Li₂CO₃ decomposition by introducing protons in a controlled and well-defined manner, and therewith substantiate our hypothesis of how Li₂CO₃ decomposes in a Li-ion battery environment?

The question on how protons can be generated in an aprotic Li-ion battery electrolyte has been posed by many researchers. In general, the formation of protons is seen to be only possible upon anodic oxidation of organic molecules or water, which is likely followed by proton abstraction [22,24,27]. As protons are intrinsically detrimental for the life-time of Li-ion batteries, leading to corrosion of cell parts [28], dissolution of the cathode active material [29,30], enhanced gassing on the counter electrode [22], and possibly decomposition of the LiPF₆ salt [24], the anodic stability of the electrolyte has always been a major leverage for achieving long cycle-life. Especially for high-voltage applications, only few solvents like some organic carbonates are sufficiently stable, while alcohols, glymes, and ethers are generally found to be unstable at elevated potentials [31]. For this reason, the purity of the solvent(s) as well as the water and HF content of the electrolyte are crucial, as we will demonstrate also later on.

To trace the formation of protons in-situ or even during operation is not trivial, but the rapid reaction of protons with PF₆⁻ (equation (4)), demonstrated by the addition of methane sulfonic acid to an EC + 1.5M LiPF₆ model electrolyte [24], can be used to indirectly trace proton formation even quantitatively. Following equation (4), every “free” proton released will readily react to form gaseous PF₅ and HF. While the latter corrodes many components in a Li-ion battery, PF₅ gas can be traced by OEMS as POF₃ at $m/z = 85$ (this is explained in detail in an earlier study by Solchenbach et al. [24]). We will make use of this indirect proton monitoring in the following experiments.

While proton formation in a pure Li-ion battery electrolyte is only occurring at high potentials and at a slow rate, a simple way of controlling the proton content in-situ is by adding a proton source to the electrolyte that only releases protons at potentials above the open-circuit potential but below the potential at which the electrolyte itself is decomposing. Such a proton source of practical relevance are alcohols, since, for example, ethylene glycol (EG) is a common impurity in standard EC-based Li-ion battery electrolytes that is formed by the slow but finite hydrolysis of ethylene carbonate (EC) when stored under imperfect conditions; thus, EG and also ethanol (EtOH) is found as trace impurity in Li-ion battery electrolytes [32,33]. Upon partial electrochemical oxidation, each OH-group of an alcohol can get converted into an aldehyde group upon the release of two protons; for example, EtOH can be electro-oxidized to acetaldehyde and two protons, while EG can be electro-oxidized to glyoxal and four protons. In aqueous acidic electrolytes, the initial oxidation of these alcohols occurs at ≈ 0.5 – 1.0 V vs the reversible hydrogen electrode (RHE) potential, which should roughly correspond to ≈ 3.5 – 4.0 V vs Li⁺/Li, whereby also higher

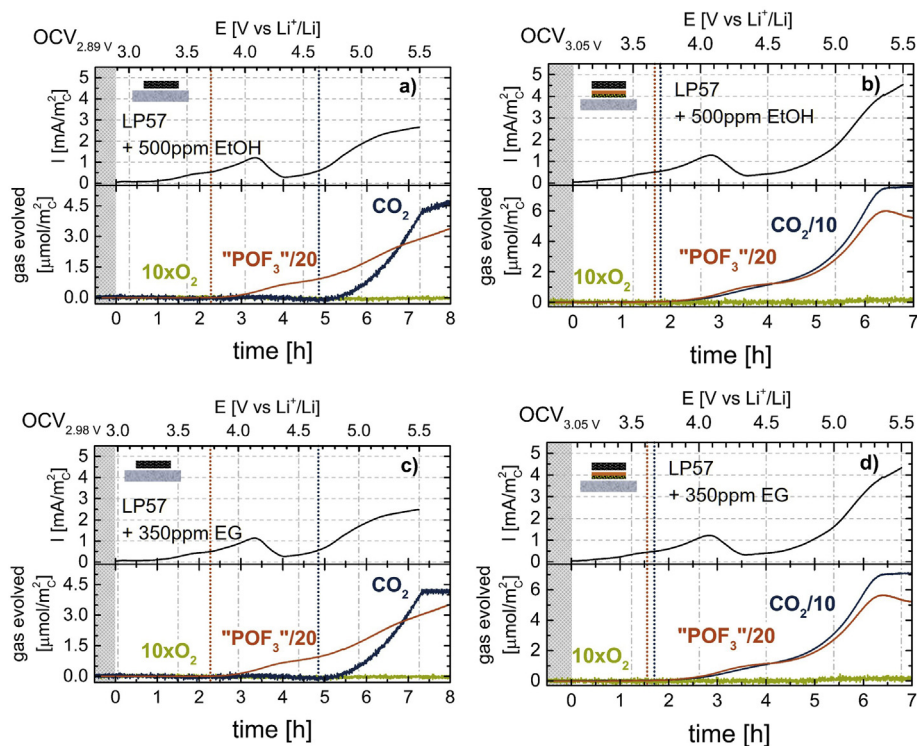


Fig. 7. Oxidation current density and gas evolution (normalized to the surface area of the C65 carbon that is in electrical contact with the C65 WE) for a linear potential scan (0.1 mV/s) of the working electrode (WE) potential from OCV (≈ 3.0 V vs Li⁺/Li) to 5.5 V vs Li⁺/Li for two different WE configurations (see sketches in the figure) with LP57 electrolyte in two-compartment OEMS cells containing alcoholic species: (a) LP57 + 500 ppm EtOH on a bare C65 WE; (b) LP57 + 500 ppm EtOH on a C65+Li₂CO₃ composite in the Li₂CO₃ interlayer configuration with a C65 WE; (c) LP57 + 350 ppm EG on a bare C65 WE; (d) LP57 + 350 ppm EG on a C65+Li₂CO₃ composite in the Li₂CO₃ interlayer configuration with a C65 WE. The anodic current is shown in the upper panels, while the cumulative amounts of evolved O₂ (green lines), CO₂ (dark blue lines), and "POF₃" (orange lines) are shown in the bottom panels. (For interpretation of the references to colour in this figure legend, the reader is referred to the Web version of this article.)

oxidation products (carboxylic acids and CO₂) can be formed [34–36], since H₂O serves as a source of oxygen. In aprotic organic electrolytes, the most likely oxidation product is the aldehyde [37]. Based on these considerations, ethylene glycol and ethanol should be viable proton sources that release protons at potentials above the OCV potential (≈ 3.0 V vs Li⁺/Li, see equation (5.1)) but well below the potential where alkyl carbonates can be oxidized (above ≈ 4.6 V vs Li⁺/Li, see equation (5.2)). Thus, we will utilize these two alcohols to examine the effect of protic impurities on the decomposition of Li₂CO₃ in a Li-ion battery environment.

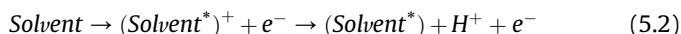
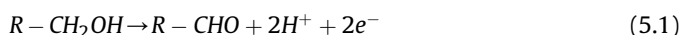


Fig. 7 combines the experiments conducted with a two-compartment OEMS cell in which the 200 μl of LP57 electrolyte that were added to the working electrode compartment were spiked with 500 ppm of EtOH or 350 ppm of EG, corresponding to the same value of ≈ 2.8 – 2.9 μmol of OH-groups. Anodic potential scans at 0.1 mV/s from OCV (≈ 3.0 V vs Li⁺/Li) to 5.5 V vs Li⁺/Li were then conducted either with the bare C65 working electrode (Fig. 7a and c) or with the C65+Li₂CO₃ composite in the Li₂CO₃ interlayer configuration (Fig. 7b and d). The m/z-trace for POF₃ is now added to the gas evolution graphs in orange; since the trace of m/z = 28 is compromised by aldehyde fragments, it can no more be used as indicator for CO and is therefore removed from further analysis. As evident from a first glance at the data, the results obtained by EtOH and EG addition are basically the same, both in terms of current vs potential and with regards to gas evolution, which is not surprising,

as the oxidation potentials of EG and EtOH are expected to be similar, and as the total moles of protons, which can be provided upon the formation of acetaldehyde and glyoxal, respectively, were chosen to be identical (see above). The results will therefore be discussed jointly, generally referring to alcoholic species.

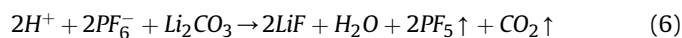
When using an electrolyte containing alcoholic species in the working electrode compartment, oxidation currents are observed at potentials as low as ≈ 3.5 V vs Li⁺/Li, with a sluggish anodic peak at ≈ 4.1 V vs Li⁺/Li, as shown in the upper panels of Fig. 7. Referencing the anodic charge associated with these currents up to ≈ 4.3 V vs Li⁺/Li to the known amount of alcoholic species in the electrolyte yields a value of $\approx 1.96 \pm 0.05$ electrons/OH-group, consistent with the electro-oxidation mechanism given in equation (5.1), by which each alcohol group is oxidized to an aldehyde group. Closely coinciding with this alcohol electro-oxidation feature, the mass traces of "POF₃" are detected by mass spectrometry (orange lines in the lower panels in Fig. 7), which we ascribe to the formation of PF₅ (detected as "POF₃" as explained in the experimental section): Please note that the scaling of the "POF₃" signal by the factor 1/20 creates the false impression that the onset potential of the "POF₃" signal might be higher than that for the anodic current. At a potential of 5.0 V vs Li⁺/Li, the amounts of "POF₃" detected in these alcohol-spiked LP57 electrolytes on a bare C65 WE (Fig. 7a and c) is ≈ 20 -fold larger than that detected in the as-received LP57 electrolyte under the same conditions (i.e., in the experiment described in Fig. 6a). In contrast to this, the onset potential and the quantity of evolved CO₂ are essentially identical for alcohol-spiked and alcohol-free LP57 electrolyte when using a bare C65 WE (compare Fig. 7a and c with Fig. 6a). In summary, the proposed anodic oxidation of the added alcohols at potentials

below ≈ 4.3 V vs Li^+/Li according to equation (5.1) is perfectly consistent with: (i) the determined ≈ 2 electrons/OH-group, (ii) the observed absence of additional CO_2 formation, and (iii) the strong PF_5 formation inferred from the “ POF_3 ” signal that indicates the formation of protons (see equation (4)). In none of the experiments shown in Fig. 7, O_2 gas evolution is observed.

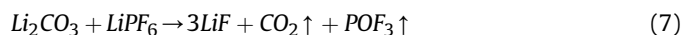
In all four experiments depicted in Fig. 7, the “ POF_3 ” signal exhibits two distinct regions, one at $\approx 3.7\text{--}4.4$ V vs Li^+/Li and one starting at ≈ 4.7 V vs Li^+/Li . The low-potential “ POF_3 ” formation region only appears upon the addition of the alcoholic species that release protons in this potential range, and it is not evident in the above discussed experiments with the pure LP57 electrolyte (those shown in Figs. 5 and 6, in which the “ POF_3 ” signal is negligible below 4.8 V vs Li^+/Li). The high-potential “ POF_3 ” formation region is largely caused by actual electrolyte oxidation, producing protons (see equation (5.2)) or protic species [22]. These will react with Li_2CO_3 to produce CO_2 and H_2O (see equation (1)), which on a time-scale of hours will react with LiPF_6 to produce POF_3 and HF (see equation (3)) [38], with the latter further decomposing any remaining Li_2CO_3 (see equation (1.2)). Thus, in case of the experiments with the C65+ Li_2CO_3 composite in the Li_2CO_3 interlayer configuration, all of the Li_2CO_3 will gradually be decomposed, accompanied by the formation of PF_5 or POF_3 , both recorded as “ POF_3 ” signal in the MS. Please note that the higher anodic currents at potentials exceeding 5.0 V vs Li^+/Li in the experiments containing the Li_2CO_3 interlayer (Fig. 7 b and d) are likely caused by the electro-oxidation of a part of the formed water that has not reacted sufficiently fast with the LiPF_6 salt (equation (3)) and that is confined in the working electrode compartment. Therefore, it is difficult to quantitatively correlate the anodic current and the CO_2 and “ POF_3 ” evolution in the high-potential “ POF_3 ” formation region. On the other hand, the “ POF_3 ” signal in the low-potential “ POF_3 ” formation region always corresponds to $\approx 17 \mu\text{mol}/\text{m}^2$ of “ POF_3 ” for the data shown in Fig. 7b and d. Since the low-potential region essentially corresponds to the potential region in which the added alcoholic species are being electro-oxidized according to equation (5.1), this also corresponds to the region where protons are being formed. Considering that the reaction of LiPF_6 with protons (equation (4)) is much faster than with water (equation (3)), as deduced from comparing the data shown in Solchenbach et al. [24] and in Strmcnik et al. [38], the “ POF_3 ” signal should correspond to PF_5 . Thus, the $\approx 17 \mu\text{mol}/\text{m}^2$ of PF_5 formed in the low-potential region would require the formation of $17 \mu\text{mol}/\text{m}^2$ of protons acc. to equation (4). As the average surface area of the C65 WE in these experiments was 0.17 m^2 , the $\approx 17 \mu\text{mol}/\text{m}^2$ of protons correspond to a total amount of $\approx 2.9 \mu\text{mol H}^+$. This is in quasi perfect agreement with the $\approx 2.8\text{--}2.9 \mu\text{mol}$ of alcoholic OH-groups in the EG or EtOH spiked LP57 electrolyte (200 μl containing 500 ppm of EtOH or 350 ppm of EG). In short, the evolved CO_2 is a quantitative measure for Li_2CO_3 decomposition by H^+ or HF, and “ POF_3 ” can be seen as a probe for LiPF_6 decomposition in the presence of H^+ .

Now that the quantitative correlation between the anodic alcohol oxidation current and the evolution of PF_5 (detected as “ POF_3 ”) is established, the important question is whether the CO_2 evolution from Li_2CO_3 decomposition is altered by the potential-dependent release of protons from the deliberately added alcoholic “impurities”. As shown in Fig. 7 b and d, the potential-dependent CO_2 evolution in the presence of the C65+ Li_2CO_3 composite in the Li_2CO_3 interlayer configuration is also exhibiting two distinct CO_2 evolution waves, overlaying very closely with the “ POF_3 ” signal. Consequently, the “ POF_3 ”: CO_2 ratio remains at an essentially constant value of close to 2:1 (observed until an anodic potential of 5.2 V vs Li^+/Li , at which point most of the Li_2CO_3 has been consumed). The overall amount of evolved CO_2 is again simply

the sum of the CO_2 released from the Li_2CO_3 interlayer and from the small background caused by anodic electrolyte oxidation on the carbon surface of the C65 WE. According to equation (1), the decomposition of 1 mol Li_2CO_3 requires 2 mol of protons. As protons instantaneously react with the LiPF_6 salt to PF_5 acc. to equation (4) (detected as “ POF_3 ” in the mass spectrometer), and as equation (1.1) can also be written with HF instead of with H^+ (see equation (1.2)), the 2:1 ratio between detected “ POF_3 ” (i.e., evolved PF_5) and CO_2 from the Li_2CO_3 decomposition is in perfect agreement with the hypothesized decomposition of Li_2CO_3 by acid attack, i.e., with the sum of equations (1.2) and (4):



The results from the alcoholic species containing electrolyte clearly reveals how Li_2CO_3 is decomposed in Li-ion battery electrolytes. As the decomposition of Li_2CO_3 in a Li-ion battery environment is releasing water (equation (1)), which over time as described in equation (3) is also forming HF, the complete decomposition of Li_2CO_3 can be seen to be a reaction that is simply catalyzed by protic species, which can be formed by either the oxidation of alcoholic impurities at low potentials (equation (5.1)) or by electrolyte oxidation at high potentials (equation (5.2)). By summing up equations (1.2) and (3), the decomposition of Li_2CO_3 can be written as:



3.4. Electro-oxidation of water in Li-ion battery electrolytes

The role of water content in Li-ion battery electrolytes has been discussed many times, especially with respect to its chemical reactivity with the electrolyte salt. Aggravated electrolyte decomposition and carbon corrosion have been observed at high potentials in Li-ion battery electrolytes spiked deliberately with water [27]. As the chemical consumption of water by the electrolyte (either due to reaction with the electrolyte salt acc. to equation (3) or due to the hydrolysis of the cyclic carbonate [32]) are slow processes at room temperature that occur on time scales on the order of hours or longer, the question arises whether water that is chemically formed upon Li_2CO_3 decomposition (via equation (1.1) or (1.2)) can itself get electro-oxidized, and thereby produce additional anodic capacity and protons. In order to answer this question, we conducted galvanostatic experiments in the one-compartment OEMS cell set-up using the same three working electrode configurations as in the one-compartment OEMS study (the bare C65 WE, the Li_2CO_3 interlayer, and the Li_2CO_3 electrode configuration) with pristine LP57 electrolyte, and then comparing these data to the galvanostatic charge of a bare C65 WE electrode with LP57 electrolyte spiked with 585 ppm of water (corresponding to the amount of water, which would be produced by the decomposition of the added amount of Li_2CO_3 acc. to equation (1.1) or (1.2)). Those four experimental cell configurations were charged galvanostatically at C/25 or at C/2 (referenced to a 2-electron decomposition mechanism of the roughly 0.60 mg Li_2CO_3 present in the cells with the Li_2CO_3 electrode or interlayer configuration) for 40 h. The potential vs time response is shown in Fig. 8.

At a C-rate of C/25 (upper panel of Fig. 8), the bare C65 WE in LP57 (dark blue) reaches a potential plateau at ≈ 5.5 V vs Li^+/Li , because at this anodic polarization the continuous electrochemical oxidation of the electrolyte is able to provide the galvanostatically applied anodic current. In accordance with the above shown results in Fig. 3, the electrochemical response of the C65/ Li_2CO_3 composite is independent of whether it is used in the electrode configuration

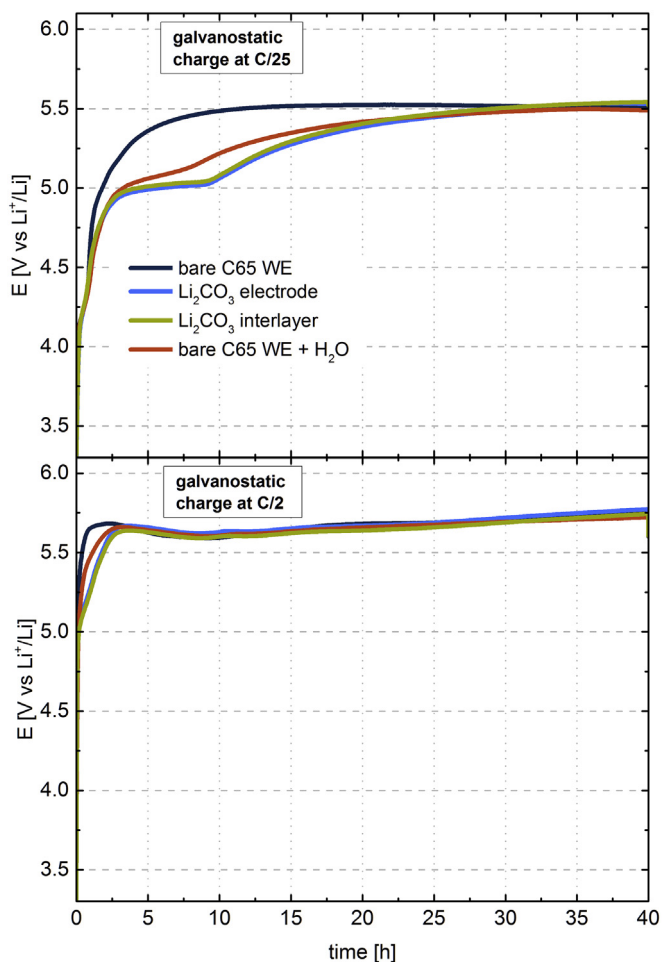


Fig. 8. Anodic polarization during galvanostatic charging (referenced to a 2-electron oxidation mechanism of the amount of Li_2CO_3 in the Li_2CO_3 electrode or interlayer configuration) at C/25 ($\equiv 0.010 \text{ mA/cm}^2$, upper panel) and C/2 ($\equiv 0.123 \text{ mA/cm}^2$, lower panel) in the one-compartment set-up with a partially delithiated LFP ($\text{Li}_{0.1}\text{FePO}_4$) CE and a polyester separator measured in LP57 on a bare C65 WE (dark blue line), a C65 WE with a Li_2CO_3 electrode (blue line), a C65 WE with Li_2CO_3 interlayer (green line), and in LP57 + 585 ppm H_2O on a bare C65 WE (orange line) for 40 h. (For interpretation of the references to colour in this figure legend, the reader is referred to the Web version of this article.)

(light blue line) or the interlayer configuration (green line). Both, however, show a plateau at $\approx 5.0 \text{ V}$ that is lasting for roughly 10–12 h, which would be the equivalent of a 1-electron process. Since the C65/ Li_2CO_3 composite in the interlayer configuration does not allow electrical contact of the Li_2CO_3 particles with the C65 WE, this charge cannot be due to the *electrochemical* oxidation of the Li_2CO_3 present in the cell, so that we ascribe the charge that is transferred in this initial lower voltage plateau to the electrochemical oxidation of H_2O formed by the chemical decomposition of Li_2CO_3 (acc. to equations (1.1) and (1.2)). In order to prove this hypothesis, the expected amount of H_2O produced by the chemical decomposition of the Li_2CO_3 present in the cells with Li_2CO_3 containing electrodes/interlayers was added to the LP57 electrolyte ($\equiv 585 \text{ ppm}$ of H_2O), with which then a cell with a bare C65 WE was charged galvanostatically at the same current density (orange line). As can be seen in Fig. 8 (upper panel), the addition of water to LP57 electrolyte also leads to an additional lower initial potential plateau centered around $\approx 5.1 \text{ V}$ that lasts for 8–10 h with a bare C65 WE, closely resembling the response of the cells with Li_2CO_3 electrode or interlayer configurations that are charged with H_2O -free LP57.

The slightly higher potential of the initial potential plateau and its slightly lower duration are, we believe, due to a reaction of the added H_2O with the electrolyte prior to starting the experiment (e.g., via equation (3)). We therefore correlate the galvanostatic charge passed during the initial potential plateau between ≈ 5.0 and $\approx 5.2 \text{ V vs Li}^+/\text{Li}$ to the electro-oxidation of H_2O . Considering that the duration of this lower potential plateau corresponds to a charge that is roughly half of that required for a 2-electron oxidation of the produced H_2O (designed to last 25 h at C/25, as described above) or of the added H_2O , the electro-oxidation of water on the C65 WE in a lithium-ion battery electrolyte must be a 1-electron process, which can be written according to equation (8).



Equation (8) is a well-known redox reaction [39–41], and the formed hydroxyl radical is highly reactive with organic electrolytes, which will lead to electrolyte decomposition and most likely additional CO_2 and CO evolution [27].

The high potentials needed to electro-oxidize water acc. to equation (8) in lithium-ion battery electrolytes is caused by the slow kinetics of this reaction, at least on bare carbon surfaces (so far we have not examined the H_2O oxidation rates on cathode active material surfaces). At the much higher C-rate of C/2 (see lower panel of Fig. 8), the water oxidation reaction is apparently not fast enough to lead to the appearance of the initial low potential plateau observed at C/25, so that the potential profiles for the four different configurations are essentially identical and are governed by the continuous electrochemical oxidation of the electrolyte. The potential sweep measurements conducted during the OEMS experiments described in the previous sections are therefore too fast to allow a distinct observation of the electro-oxidation of the water formed by the chemical decomposition of the Li_2CO_3 . Electro-oxidation of water on transition metal oxide surfaces could be favored and could therefore happen at lower overpotentials, but this question is beyond the scope of this study.

3.5. Summary of the Li_2CO_3 decomposition mechanism and the follow-up reactions

The full mechanism based on the results obtained in this study is shown in Fig. 9: Li_2CO_3 is decomposed by a purely *chemical* reaction to form H_2O and CO_2 according to equation (1.1) or (1.2). This reaction is initiated by “free” protons formed upon the anodic oxidation of the electrolyte solvent at high potentials ($>4.6 \text{ V vs Li}^+/\text{Li}$) or of alcoholic electrolyte impurities at already very low potentials (ca. $>3.5 \text{ V vs Li}^+/\text{Li}$), but also by high HF content of the electrolyte which can result from the intrusion of trace water impurities that on the time-scale of 5–20 h produces HF [38] (see equation (3)). Protons instantaneously react with the PF_6^- anion of the conductive LiPF_6 salt, forming HF and PF_5 gas, whereby the latter can be traced quantitatively by OEMS. HF reacts with Li_2CO_3 according to equation (1.2). While the water formed by the decomposition of Li_2CO_3 could act as an additional proton source at high anodic potentials, its chemical reaction with LiPF_6 to POF_3 , LiF , and HF (equation (3)) is more likely to occur in a Li-ion battery with conventionally used upper cutoff potential limits of $<4.6 \text{ V vs Li}^+/\text{Li}$, but on a time-scale of 5–20 h. Another chemical sink for H_2O in the electrolyte, the hydrolysis reaction with particularly cyclic carbonate solvents, will lead to alcohol groups (e.g., ethylene glycol from EC) [32] that will oxidize at already $\approx 3.5 \text{ V vs Li}^+/\text{Li}$ and thereby release protons during anodic polarization well within the operation window of a Li-ion battery.

Finally, considering the effect of this reaction cascade for an operating Li-ion battery employing a mixed transition metal

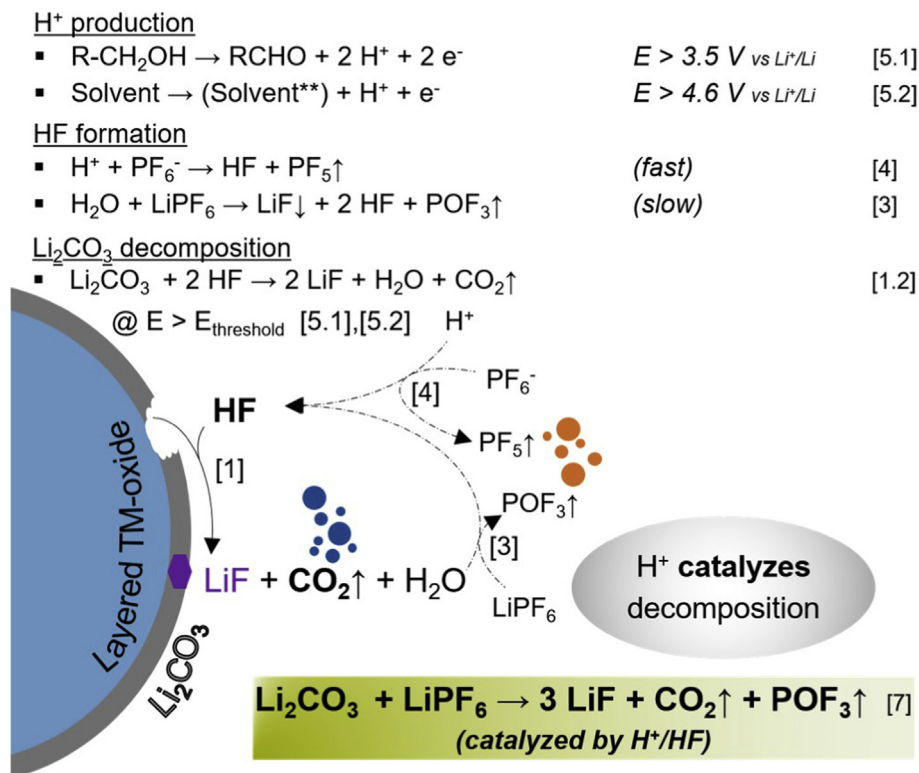


Fig. 9. Scheme of Li₂CO₃ decomposition in the Li-ion battery environment, showing the governing reaction equations discussed in the text. Protons catalyse the decomposition of Li₂CO₃, whereas their formation strongly depends on the purity and kind of solvents used.

layered oxide, the most dominant impact is the reaction of the active material with the formed HF, leading to material loss by transition metal dissolution that increases the impedance on the positive and negative electrode. A secondary effect is that the corrosion of particularly the aluminum current-collector at the cathode by HF will further increase the internal resistance of the cell through the formation of a significant contact resistance at the aluminum/cathode electrode interface [28]. While the reaction cascade is initiated by the first protons formed, which is only dependent on the purity of the electrolyte with respect to HF, alcoholic impurities, and any residual water, it will proceed according to equation (7) until all the Li₂CO₃ present in the cell has been consumed. Thus, Li₂CO₃ impurities introduced into the cell mostly via layered oxide based cathode active materials can release water over a prolonged time-scale, particularly if the solid electrolyte interphase on anode electrode is already stable enough to prevent H₂O and HF from being scavenged from the electrolyte by cathodic reduction. Aggravated cell aging of positive electrode materials containing significant amount of Li₂CO₃ can therefore be expected, in addition to the fact that it will lead to cell bulging [7,12].

4. Conclusions

In this work, we have studied the decomposition mechanism of Li₂CO₃ in the Li-ion battery environment. Experiments with model electrodes composed of conductive carbon and Li₂CO₃ clearly demonstrated the high relevance of Li₂CO₃ impurities for Li-ion batteries employing layered transition metal oxide based cathode active materials. Particularly Ni-rich layered transition metal oxides are prone to have large Li₂CO₃ surface impurities that form both during their preparation and upon exposure to ambient air.

We showed in detail that the decomposition of Li₂CO₃ in organic carbonate solvents does not occur through an *electrochemical* oxidation reaction, but that it occurs exclusively through a purely *chemical* decomposition reaction that is triggered by protic species formed upon the anodic oxidation of organic solvents at >4.6 V vs Li⁺/Li, by trace water, or by HF impurities.

While the extent to which Li₂CO₃ decomposition is completed within the first anodic polarization of the positive electrode is dependent on the electrolyte and its purity, the complete decomposition of all Li₂CO₃ contained in the cell will inevitably occur, since the water formed by the chemical Li₂CO₃ decomposition reaction will gradually form HF due to reaction with the LiPF₆ conducting salt. Li₂CO₃ decomposition is a process catalyzed by the first protic species that are formed in the electrolyte, so that all Li₂CO₃ in the cell will be consumed completely over time. This reaction cascade can only be interrupted by proton-scavenging additives or by the reductive removal of water and HF on the anode prior to the formation of a stable SEI. The amount of CO₂ formed upon Li₂CO₃ decomposition can lead to cell bulging, if significant amounts of Li₂CO₃ are still present after the degassing step during formation.

Furthermore, we have shown that alcoholic impurities in Li-ion battery electrolytes oxidize electrochemically at already >3.5 V vs Li⁺/Li, leading to a quantitative release of protons. These rapidly react with LiPF₆ to HF, which in turn will lead to the known aging mechanisms, such as corrosion of the metallic cell parts and leaching of transition metals from the active material.

Declaration of competing interest

The authors declare that they have no known competing financial interests or personal relationships that could have

appeared to influence the work reported in this paper.

CRedit authorship contribution statement

Anna T.S. Freiberg: Methodology, Investigation, Writing - original draft. **Johannes Sicklinger:** Investigation, Writing - review & editing. **Sophie Solchenbach:** Methodology, Writing - review & editing. **Hubert A. Gasteiger:** Conceptualization, Supervision, Writing - review & editing.

Acknowledgement

Financial support by BASF SE through its Scientific Network on Electrochemistry and Batteries is gratefully acknowledged. Further gratitude is expressed to Dr. Hany El-Sayed for TEM images and Franziska Friedrich for the XRD measurements.

References

- [1] G.E. Blomgren, The development and future of lithium ion batteries, *J. Electrochem. Soc.* 164 (2016) A5019–A5025.
- [2] O. Gröger, H.A. Gasteiger, J.-P. Suchsland, Review—electromobility: batteries or fuel cells? *J. Electrochem. Soc.* 162 (2015) A2605–A2622.
- [3] S.-T. Myung, F. Maglia, K.-J. Park, C.S. Yoon, P. Lamp, S.-J. Kim, Y.-K. Sun, Nickel-rich layered cathode materials for automotive lithium-ion batteries: achievements and perspectives, *ACS Energy Letters* 2 (2017) 196–223.
- [4] H.-J. Noh, S. Yoon, C.S. Yoon, Y.-K. Sun, Comparison of the structural and electrochemical properties of layered $\text{Li}[\text{Ni}_x\text{Co}_y\text{Mn}_z]\text{O}_2$ ($x = 1/3, 0.5, 0.6, 0.7, 0.8$ and 0.85) cathode material for lithium-ion batteries, *J. Power Sources* 233 (2013) 121–130.
- [5] J. Sicklinger, M. Metzger, H. Beyer, D. Pritzl, H.A. Gasteiger, Ambient storage derived surface contamination of NCM811 and NCM111: performance implications and mitigation strategies, *J. Electrochem. Soc.* 166 (2019) A2322–A2335.
- [6] I.A. Shkrob, J.A. Gilbert, P.J. Phillips, R. Klie, R.T. Haasch, J. Bareño, D.P. Abraham, Chemical weathering of layered Ni-rich oxide electrode materials: evidence for cation exchange, *J. Electrochem. Soc.* 164 (2017) A1489–A1498.
- [7] R. Jung, R. Morasch, P. Karayaylali, K. Phillips, F. Maglia, C. Stinner, Y. Shao-Horn, H.A. Gasteiger, Effect of ambient storage on the degradation of Ni-rich positive electrode materials (NMC811) for Li-ion batteries, *J. Electrochem. Soc.* 165 (2018) A132–A141.
- [8] G.V. Zhuang, G. Chen, J. Shim, X. Song, P.N. Ross, T.J. Richardson, Li_2CO_3 in $\text{LiNi}_0.8\text{Co}_0.15\text{Al}_0.05\text{O}_2$ cathodes and its effects on capacity and power, *J. Power Sources* 134 (2004) 293–297.
- [9] S.S. Zhang, Insight into the gassing problem of Li-ion battery, *Frontiers in Energy Research* 2 (2014).
- [10] N.V. Faenza, Z.W. Lebens-Higgins, P. Mukherjee, S. Sallis, N. Pereira, F. Badway, A. Halajko, G. Ceder, F. Cosandey, L.F.J. Piper, G.G. Amatucci, Electrolyte-induced surface transformation and transition-metal dissolution of fully delithiated $\text{LiNi}_0.8\text{Co}_0.15\text{Al}_0.05\text{O}_2$, *Langmuir* (2017).
- [11] D. Pritzl, T. Teufel, A.T.S. Freiberg, B. Strehle, J. Sicklinger, H. Sommer, P. Hartmann, H.A. Gasteiger, Washing of nickel-rich cathode materials for lithium-ion batteries: towards a mechanistic understanding, *J. Electrochem. Soc.* 166 (2019) A4056–A4066.
- [12] Y. Bi, T. Wang, M. Liu, R. Du, W. Yang, Z. Liu, Z. Peng, Y. Liu, D. Wang, X. Sun, Stability of Li_2CO_3 in cathode of lithium ion battery and its influence on electrochemical performance, *RSC Adv.* 6 (2016) 19233–19237.
- [13] S. Yang, P. He, H. Zhou, Exploring the electrochemical reaction mechanism of carbonate oxidation in Li-air/ CO_2 battery through tracing missing oxygen, *Energy Environ. Sci.* 9 (2016) 1650–1654.
- [14] N. Mahne, S.E. Renfrew, B.D. McCloskey, S.A. Freunberger, Electrochemical oxidation of lithium carbonate generates singlet oxygen, *Angew. Chem. Int. Ed. Engl.* 57 (19) (2018) 5529–5533, <https://doi.org/10.1002/anie.201802277>.
- [15] S. Meini, N. Tsiouvaras, K.U. Schwenke, M. Piana, H. Beyer, L. Lange, H.A. Gasteiger, Rechargeability of Li-air cathodes pre-filled with discharge products using an ether-based electrolyte solution: implications for cycle-life of Li-air cells, *Phys. Chem. Chem. Phys.* 15 (2013) 11478.
- [16] J. Wandt, P. Jakes, J. Granwehr, H.A. Gasteiger, R.-A. Eichel, Singlet oxygen formation during the charging process of an aprotic lithium-oxygen battery, *Angew. Chem. Int. Ed.* 55 (2016) 6892–6895.
- [17] N. Mahne, B. Schafzahl, C. Leybold, M. Leybold, S. Grumm, A. Leitgeb, Gernot A. Strohmeyer, M. Wilkening, O. Fontaine, D. Kramer, C. Slugovc, Sergey M. Borisov, Stefan A. Freunberger, Singlet oxygen generation as a major cause for parasitic reactions during cycling of aprotic lithium-oxygen batteries, *Nature Energy* 2 (2017) 17036.
- [18] A.T.S. Freiberg, M.K. Roos, J. Wandt, R. de Vivie-Riedle, H.A. Gasteiger, Singlet oxygen reactivity with carbonate solvents used for Li-ion battery electrolytes, *J. Phys. Chem.* 122 (2018) 8828–8839.
- [19] P.R. Ogilby, C.S. Foote, Chemistry of singlet oxygen. 42. Effect of solvent, solvent isotopic substitution, and temperature on the lifetime of singlet molecular oxygen ($^1\Delta_g$), *J. Am. Chem. Soc.* 105 (1983) 3423–3430.
- [20] J. Wandt, A.T.S. Freiberg, A. Ogrodnik, H.A. Gasteiger, Singlet oxygen evolution from layered transition metal oxide cathode materials and its implications for lithium-ion batteries, *Mater. Today* 21 (2018) 825–833.
- [21] T. Bartsch, F. Strauss, T. Hatsukade, A. Schiele, A.Y. Kim, P. Hartmann, J. Janek, T. Brezesinski, Gas evolution in all-solid-state battery cells, *ACS Energy Letters* 3 (2018) 2539–2543.
- [22] M. Metzger, B. Strehle, S. Solchenbach, H.A. Gasteiger, Origin of H_2 evolution in LIBs: H_2O reduction vs. Electrolyte oxidation, *J. Electrochem. Soc.* 163 (2016) A798–A809.
- [23] S.E. Renfrew, B.D. McCloskey, The role of electrolyte in the first-cycle transformations of $\text{LiNi}_0.6\text{Mn}_0.2\text{Co}_0.2\text{O}_2$, *J. Electrochem. Soc.* 166 (2019) A2762–A2768.
- [24] S. Solchenbach, M. Metzger, M. Egawa, H. Beyer, H.A. Gasteiger, Quantification of PF_5 and POF_3 from side reactions of LiPF_6 in Li-ion batteries, *J. Electrochem. Soc.* 165 (2018) A3022–A3028.
- [25] N. Tsiouvaras, S. Meini, I. Buchberger, H.A. Gasteiger, A novel on-line mass spectrometer design for the study of multiple charging cycles of a Li- O_2 battery, *J. Electrochem. Soc.* 160 (2013) A471–A477.
- [26] H. Beyer, S. Meini, N. Tsiouvaras, M. Piana, H.A. Gasteiger, Thermal and electrochemical decomposition of lithium peroxide in non-catalyzed carbon cathodes for Li-air batteries, *Phys. Chem. Chem. Phys.* 15 (2013) 11025.
- [27] M. Metzger, C. Marino, J. Sicklinger, D. Haering, H.A. Gasteiger, Anodic oxidation of conductive carbon and ethylene carbonate in high-voltage Li-ion batteries quantified by on-line electrochemical mass spectrometry, *J. Electrochem. Soc.* 162 (2015) A1123–A1134.
- [28] D. Pritzl, A.E. Bumberger, M. Wetjen, J. Landesfeind, S. Solchenbach, H.A. Gasteiger, Identifying contact resistances in high-voltage cathodes by impedance spectroscopy, *J. Electrochem. Soc.* 166 (2019) A582–A590.
- [29] D.R. Gallus, R. Schmitz, R. Wagner, B. Hoffmann, S. Nowak, I. Cekic-Laskovic, R.W. Schmitz, M. Winter, The influence of different conducting salts on the metal dissolution and capacity fading of NCM cathode material, *Electrochim. Acta* 134 (2014) 393–398.
- [30] N.P.W. Pieczonka, Z. Liu, P. Lu, K.L. Olson, J. Moote, B.R. Powell, J.-H. Kim, Understanding transition-metal dissolution behavior in $\text{LiNi}_0.5\text{Mn}_1.5\text{O}_4$ high-voltage spinel for lithium ion batteries, *J. Phys. Chem. C* 117 (2013) 15947–15957.
- [31] K. Xu, Nonaqueous liquid electrolytes for lithium-based rechargeable batteries, *Chem. Rev.* 104 (2004) 4303–4417.
- [32] M. Metzger, B. Strehle, S. Solchenbach, H.A. Gasteiger, Hydrolysis of ethylene carbonate with water and hydroxide under battery operating conditions, *J. Electrochem. Soc.* 163 (2016) A1219–A1225.
- [33] U. Heider, R. Oesten, M. Jungnitz, Challenge in manufacturing electrolyte solutions for lithium and lithium ion batteries quality control and minimizing contamination level, *J. Power Sources* 81–82 (1999) 119–122.
- [34] G. Horányi, V.E. Kazarinov, Y.B. Vassiliev, V.N. Andreev, Electrochemical and adsorption behaviour of ethylene glycol and its oxidative derivatives at platinum electrodes, *J. Electroanal. Chem. Interfacial Electrochem.* 147 (1983) 263–278.
- [35] B. Wieland, J.P. Lancaster, C.S. Hoaglund, P. Holota, W.J. Tornquist, Electrochemical and infrared spectroscopic quantitative determination of the platinum-catalyzed ethylene glycol oxidation mechanism at CO adsorption potentials, *Langmuir* 12 (1996) 2594–2601.
- [36] M.R. Tarasevich, O.V. Korchagin, A.V. Kuzov, Electrocatalysis of anodic oxidation of ethanol, *Russ. Chem. Rev.* 82 (2013) 1047–1065.
- [37] H.A. El-Sayed, V.M. Burger, M. Miller, K. Wagenbauer, M. Wagenhofer, H.A. Gasteiger, Ionic conductivity measurements—A powerful tool for monitoring polymer reduction reactions, *Langmuir* 33 (2017) 13615–13624.
- [38] D. Strmcnik, I.E. Castelli, J.G. Connell, D. Haering, M. Zorko, P. Martins, P.P. Lopes, B. Genorio, T. Østergaard, H.A. Gasteiger, F. Maglia, B.K. Antonopoulos, V.R. Stamenkovic, J. Rossmeisl, N.M. Markovic, Electro-catalytic transformation of HF impurity to H_2 and LiF in lithium-ion batteries, *Nature Catalysis* 1 (2018) 255–262.
- [39] F.D. Coms, H. Liu, J.E. Owejan, Mitigation of Perfluorosulfonic Acid Membrane Chemical Degradation Using Cerium and Manganese Ions, vol. 16, 2008, pp. 1735–1747.
- [40] E. Endoh, Development of highly durable PFSA Membrane and MEA for PEMFC under high temperature and low Humidity Conditions, vol. 16, 2008, pp. 1229–1240.
- [41] E. Endoh, Highly durable perfluorosulfonic acid membranes, in: H.A. Gasteiger, W. Vielstich, H. Yokokawa (Eds.), *Handbook of Fuel Cells*, John Wiley & Sons, Chichester, 2009, pp. 361–374.